Photochromic naphthopyran dyes incorporating a benzene, thiophene or furan spacer: effect on photochromic, optoelectronic and photovoltaic properties in dye-sensitized solar cells.

*Johan Liotier, Valid Mwatati Mwalukuku, Samuel Fauvel, Antonio J. Riquelme, Juan A. Anta, Pascale Maldivi and Renaud Demadrille**

J. Liotier, V. M. Mwalukuku, P. Maldivi, R. Demadrille
Univ. Grenoble Alpes, CEA, CNRS, IRIG-SyMMES, 38000 Grenoble, France
E-mail: renaud.demadrille@cea.fr

A. J. Riquelme, J. A. Anta
Área de Química Física, Universidad Pablo de Olavide, E-41013 Seville, Spain

Keywords: (photochromic dyes, organic dyes, photosensitizer, photovoltaic, solar cells, DSSC)

Abstract

We recently demonstrated that diaryl-naphthopyran photochromic dyes are efficient for sensitization of TiO_2 mesoporous electrodes, thus allowing the fabrication of photo-chromo-voltaic cells that can self-adapt their absorption of light and their generation of electricity with the light intensity. Herein we report the synthesis, the characterisation of two novel photochromic dyes based on diaryl-naphthopyran core i.e NPI-ThPh and NPI-FuPh for use in Dye Sensitized Solar Cells (DSSCs). Compared to our reference dye NPI, the molecules only vary by the nature of the spacer, a thiophene or a furan, connecting the photochromic unit and the phenyl-cyano-acrylic acid moiety used as the anchoring function. We found that swapping a phenyl for a thiophene or a furan leads to an improvement of the absorption properties of the molecules both in solution and after grafting on TiO_2 electrodes, however their photochromic process becomes not fully reversible. Despite better absorption in the visible range, the new dyes show poorer photochromic and photovoltaic properties in devices compared to NPI. Thanks to UV-Vis spectroscopy, DFT calculation, electrical characterization of the cells, and impedance spectroscopy, we unravel the factors limiting their performances. Our study

contributes to better understand the connection between photochromic and photovoltaic properties, which is key to develop better performing molecules of this class.

1. Introduction

In the last decades, the world's energy needs have been growing steadily as our lifestyles and industrial development have evolved. In 60 years, primary energy consumption has increased fourfold worldwide, and today, this energy is mainly of fossil origin. The use of these carbon sources is responsible for the emission of greenhouse gas and fine particles, with adverse effects on the climate, the environment and human health. Climate changes will affect energy systems globally and at the regional scale.[1] To reduce greenhouse gas emissions, with the goal to limit the rise in temperature to below +2°C compared to the pre-industrial era, it will be mandatory to increase the use of renewable energies. Among the renewable energy sources, photovoltaic technologies can be an asset to tackle this challenge. However today it is urgent to develop efficient and low-cost photovoltaic technologies that can be implemented everywhere, including in less sunny environments.[2]

Among photovoltaic technologies capable to comply with these criteria, dye-sensitized solar cells (DSSCs) show a great potential. Under full sun illumination (standard AM1.5G), at the laboratory scale, they demonstrate a power conversion efficiency (PCE) of 13% (certified value) and small modules can attain PCE comprised between 8 and 10%.[3,4] DSSCs show remarkable performance under various inclinations and irradiation conditions. In particular, under artificial light sources they can reach PCE over 30 %.[5–7] Compared to other emerging PV technologies, another strong advantage of DSSCs rely on their stability that has been demonstrated equivalent to 10 years of outdoor operation.[8,9] From the industrial point of view, DSSCs manufacturing process is simple and compatible with large-scale production. DSSCs can also be semi-transparent and colourful; their optical properties are fully

customizable allowing reconciling aesthetic features with energy production.[8] This last advantage is particularly appealing for applications in BIPV and automobile.[10–12]

However, when developing semi-transparent solar cells for integration in building as windows, a trade-off between the transparency and efficiency of the cells has to be found. To reach a high level of transparency the efficiency has often to be sacrificed.[13]

Another drawback of semi-transparent solar cells is related to their optical transmission that is fixed during the fabrication process. Consequently, their light transmission cannot adapt with the lighting conditions and the lack of visual comfort for the users can limit their potential of integration as photovoltaic windows in buildings.

Recently, we developed a new class of photochromic photosensitizers to tackle this problem.[14] These photochromic photosensitizers can advantageously be employed in dye-sensitized solar cells to give rise to a novel class of semi-transparent photovoltaic devices that self-adjust their optical properties to the irradiation conditions. We demonstrated that organic dyes embedding a diphenyl-naphthopyran unit can switch from a non-coloured state (closed) to a coloured state (open) on mesoporous TiO_2 electrode and photosensitized this semiconductor. We found that photochromic dyes incorporating an indenonaphthalene unit, as **NPI**, show the best performances in solar cells with a PCE above 4.1%.[14] However, to boost the efficiency of this new class of dyes in solar cells it would be desirable to improve the absorption of the open form of the photochromic molecule generated under illumination. One strategy to achieve this goal would be to modify the photochromic unit by replacing one of the phenyl ring borne in positions 2 and 2' by aromatic heterocycles. The introduction of electron-rich units such as thiophene in the 2,2' position was demonstrated to significantly increase the colorability of the molecule under irradiation in 3H-naphthopyran series.[15] The introduction of aromatic heterocycles such as thiophene is not only interesting from the point of view of photochromic properties, but also very relevant from the photosensitisation point of view. Indeed, the introduction of thiophene units in a classical dye structure has already

been reported. It was showed that the molar absorption coefficient of the thiophene containing dyes is higher and that this chemical modification leads to an increase in cell performances.[16] Another alternative to modulate the properties of these compounds would be to use furans. Indeed, furan has been incorporated into the structure of classical dyes for DSSC applications several times leading to similar effects as thiophene on the optical properties, allowing to increase the range of absorption and molar absorption coefficients.[4,17–19] Tuning of π-spacers has been proved to be a powerful strategy to tune the opto-electronic properties and performances of classical dyes, it appeared relevant if such approach could be efficient with photochromic dyes.[20]

Therefore, in this work, we report the replacement of one of the phenyl substituents of the diphenyl-naphthopyran photochromic unit by a thiophene or a furan. We synthesized two new compounds **NPI-ThPh** and **NPI-FuPh** that were compared to **NPI**, our reference dye. We investigated the effect of this structure modification on the photochromic and optoelectronic properties of the dyes as well as the impact on their photovoltaic performances in dye solar cells. We highlight that design rules established to improve the performances of classical organic photosensitizers in DSSC cannot be directly applied to photochromic dyes. Our study contributes to understand better the relationships between photochromic and photovoltaic properties within this novel class of multifunctional dyes. The structure properties relationships that we established through this work will be useful for future developements of photochromic photosensitizers.

2. Results and discussion

2.1. Design and synthesis

On the basis of our previous work, we selected the molecule **NPI** to investigate chemical modifications with the goal to establish new structure-properties relationships and design rules for this class of dyes.

To improve the optical properties of this photochromic photosensitizer, a new synthetic approach was developed to incoporate a thiophene or furan unit linked to the naphtopyran ring and connecting the spacer bearing the anchoring function. In the case of naphthopyran dyes, the use of such modifications can also have an effect on the photochromic properties. The introduction of a thiophene unit has already been reported on naphthopyrans showing a modification on the absorption of the dye in the coloured state and the discoloration kinetic.[15,21] Two new dyes were synthesized and characterised, **NPI-ThPh** and **NPI-FuPh**.

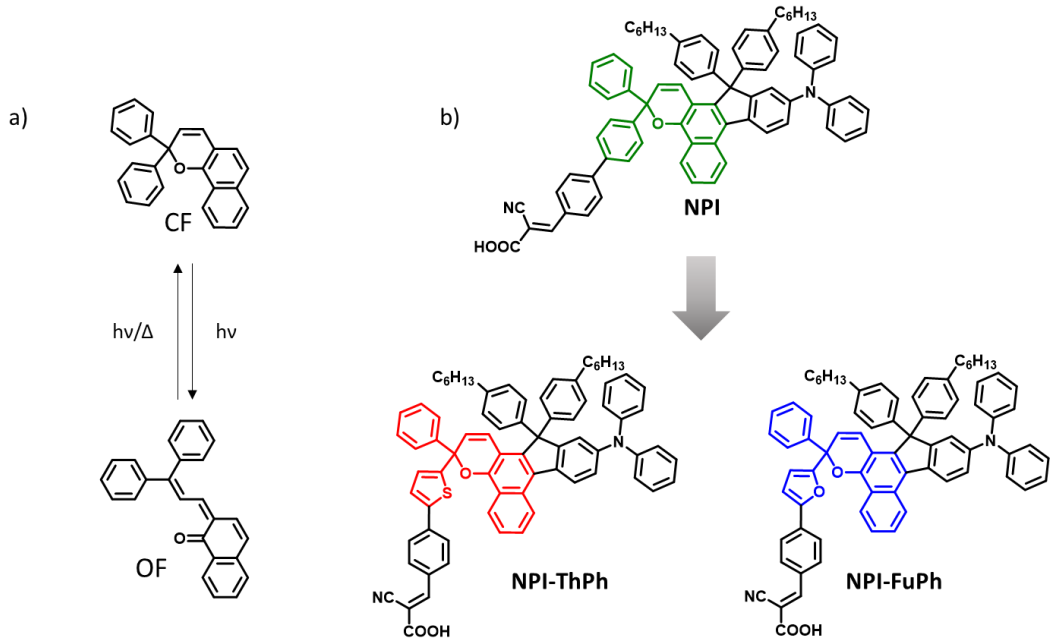

Figure 1. a) Isomerisation of 2,2'-diphenyl-[2*H*]-naphtho[1,2-*b*]pyran dye upon irradiation; b) Molecular structure from NPI and of the two new derivatives presented in this work NPI-ThPh and NPI-FuPh

The synthesis route to access to the new dyes is reported in Figure 2. The synthesis of these molecules is partly convergent and relies on the preparation of different synthons. The first

one is the naphthol precursor **10**, this building block is common for the three dyes and its preparation was reported in our previous work.[14] The other precursors are propargylic alcohols **6**, **7** and **8** containing a phenyl, a thiophene or a furan unit. These molecules are obtained from the molecules **1**, **2** and **3**. The ketone **1** is a commercial compound whereas the synthesis of the ketones **2** and **3** have to be prepared and their synthesis is presented in the supporting information. Compound **2** is obtained by Friedel-Crafts reaction between benzoyl chloride and bromothiophene.[22] For compound **3**, the Friedel-Crafts reaction between benzoyl chloride and bromofuran did not lead to the expected product. The alternative synthetic route chosen was the addition of phenyl magnesium bromide on 5-bromofuran-2-carbaldehyde.[23] These molecules are then coupled with the 2-(4-(5,5-dimethyl-1,3-dioxan-2-yl)phenyl)-4,4,5,5-tetramethyl-1,3,2-dioxaborolane *via* a Suzuki Pd-catalyzed cross-coupling with $Pd(dppf)Cl_2$ as catalyst to give compounds **4**, **5**, and **6**. The desired propargylic alcohols are then obtained by addition of ((trimethylsilyl)ethynyl)lithium on the ketones. The trimethylsilylacetylene is then deprotected with a NaOH methanol solution in the case of the compounds **7** and **8** and by TBAF in the case of **9**. For this last compound, TBAF was chosen instead of NaOH to avoid a degradation of the furan moiety. The different synthons are then condensed *via* a chromenisation reaction catalysed with PPTS in presence of $HC(OMe)_3$. The photochromic intermediates bearing the protected aldehyde are then treated with a solution of HCl (6M) to obtain the compounds **11**, **12** and **13**. The final products **NPI**, **NPI-ThPh** and **NPI-FuPh** are then obtained via a Knoevenagel reaction with cyanoacetic acid.

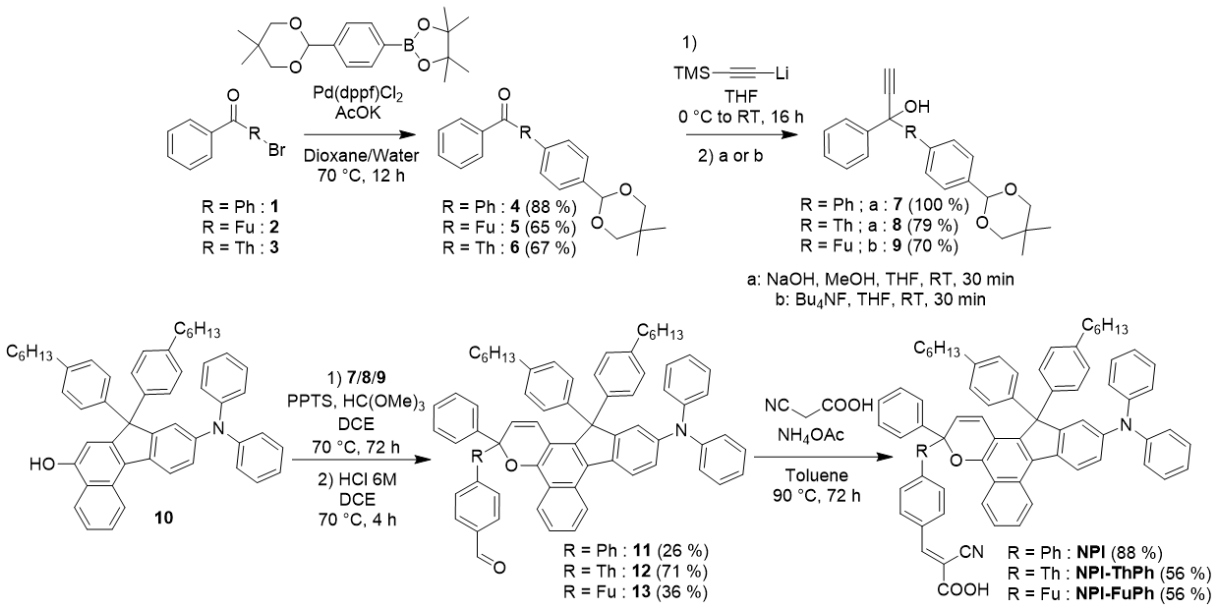

Figure 2. Synthetic pathway to obtain **NPI**, **NPI-ThPh** and **NPI-FuPh**.

2.2. Optoelectronic properties

2.2.1. UV-Vis spectroscopy and energy levels

The three products were analyzed by UV-Vis spectroscopy in toluene solution at a concentration of 2.10^{-5} M. The spectra of closed and opened forms are presented alongside with the thermal discoloration kinetics in the **Figure 3** and the optical parameters are resumed in the **Table 1**. The new compounds show a photochromic behaviour in solution, upon irradiation of the ring-closed form, the cleavage of the C-O bond of the pyranic moiety gives rise to a rearrangement of the π-conjugated system and the open-form isomers are formed. The coloured isomers show a large and intense absorption band in the visible range. One can observe that contrarily to **NPI**, the solutions of **NPI-ThPh** and **NPI-FuPh** show a weak absorption band in the visible range even when they are analysed in the dark, indicating the presence of open form species. In the case of **NPI-ThPh** and **NPI-FuPh**, under irradiation, the introduction of an electron rich unit like the thiophene or the furan induces a bathochromic shift of the absorption band compared to the **NPI** dye (whose λ_{max} is located at 605 nm) with an absorption band edge that reaches the NIR region. This spectral modification is

concomitent with a hyperchromic effect. For **NPI-ThPh**, the bathochromic shift of the absorption band of the coloured isomers in the visible is of 37 nm with a λ_{max} located at 642 nm. The hyperchromic effect for this molecule corresponds to an augmentation of the absorption of 250 % at the photostationary state (PSS) compared to **NPI**. For **NPI-FuPh** a shift of 50 nm is observed for the λ_{max} that is found at 655 nm and an increase of the absorption of 130 % is measured at the PSS in comparison to **NPI**. The introduction of furan or thiophene units whose resonance energies are lower than the ones of the benzene facilitates π-orbital overlap via the quinoid resonance structure in the open form isomers and produces consequent red-shift of their absorption.[24] The bathochromic shifts of the absorption band of the coloured isomers for **NPI-FuPh** and **NPI-ThPh** are in good agreement with previous observations on conventional dyes[25]

Under illumination the PSS was rapidly reached (< 60 s at 25 °C), the irradiation was turned off and the decolouration curves were registered and modelled using the following equation where, A(t) is the absorbance of the solution, k is the thermal decolouration kinetic constant (in s^{-1}) of the kinetic process, a_1 is the amplitude of the kinetics of this process, and A_∞ is the residual absorbance.

$$A(t) = a_1 e^{-k_1 t} + A_\infty$$

From the curves in **Figure 3b**, it appears that the thermal kinetic constant of discoloration is greatly affected by the modification of the aryl moiety. The kinetic passes from 2.08 10^{-3} s^{-1} for **NPI** to 1.45 10^{-3} s^{-1} for **NPI-ThPh** and 1.31 10^{-3} s^{-1} for **NPI-FuPh**. However, the most striking observation is that swapping a phenyl for a thiophene or a furan strongly stabilizes the opened form isomers in solution, the residual absorbance A_∞ (see non-normalized curves presented in ESI) is 0.14 for **NPI-ThPh** and 0.22 for **NPI-FuPh**. This residual coloration is not due to the formation of degradation products, as confirmed by NMR spectroscopy, it is clearly related to the formation of persistent coloured isomers.

With the goal to evaluate the effect of visible light on the stability of the open form isomers, the discoloration curves of NPI-ThPh and NPI-FuPh were recorded under illumination with visible light using a filter allowing the photons in the 550-650 nm window to pass. These experiments show that the decolouration is faster when using selectively visible light, the discolouration kinetics are accelerated by 21.4% and 51.9% for **NPI-ThPh** and **NPI-FuPh** respectively. However, even under those conditions the bleaching is not complete. To understand the persistence of the coloured isomers, a DFT study was carried out (see next section).

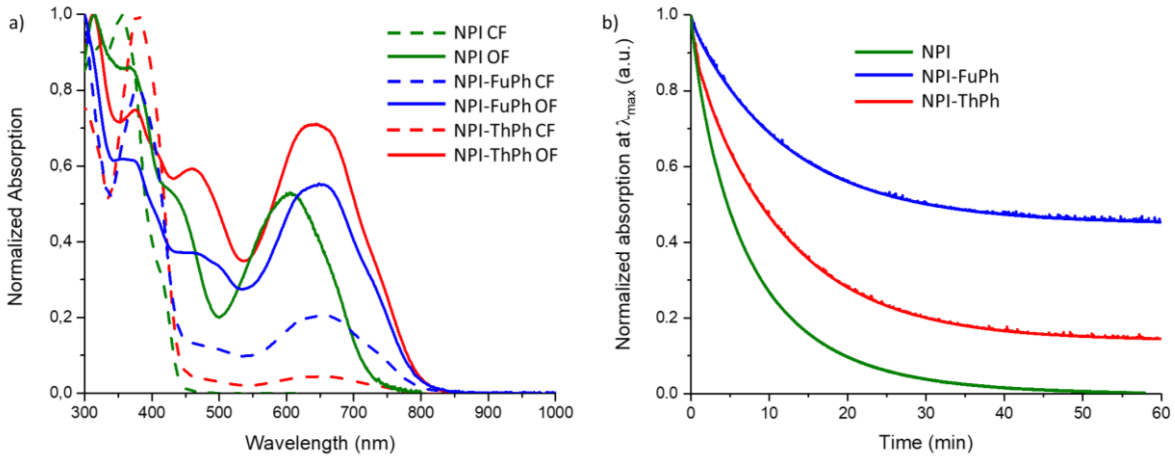

Figure 3. a) Absorption spectra of **NPI** (green), **NPI-FuPh** (blue) and **NPI-ThPh** (red) before (dashed line) and after (plain line) irradiation; b) Normalized discoloration kinetics of **NPI**, **NPI-FuPh** and **NPI-ThPh**. (Toluene, 2.10^{-5} M, 25 °C, Irradiation: 200 W, 300-600 nm).

Table 1. Optical properties of the three dyes. ΔE_{opt} OF corresponds to the optical band gap of the opened form; k is the kinetic constant of the mono-exponential modelling of the discoloration; A_{eq} corresponds to the absorption intensity observed at the PSS and A_∞ is the absorption obtained after a long time of discoloration.

Dye	λ_{max} CF [nm]	λ_{onset} CF [nm]	λ_{max} OF [nm]	λ_{onset} OF [nm]	ΔE_{opt} OF [eV]	K [s^{-1}]	A_{eq}	A_∞
NPI	318	450	605	728	1.70	$2.08.10^{-3}$	0.38	0
NPI-ThPh	378	450	642	798	1.55	$1.45.10^{-3}$	0.97	0.14
NPI-FuPh	380	450	655	800	1.55	$1.31.10^{-3}$	0.49	0.22

Finally, cyclic voltammetry measurements were carried out in the dark and under illumination in dichloromethane solution for the three dyes with the goal to determine the energy levels of their frontier orbitals (see ESI). We confirmed through these experiments that, as for **NPI**, the

two novel dyes both in their closed and opened forms can inject electrons into the TiO_2 conduction band located at around -4.1 eV, since their lowest unoccupied molecular orbital (LUMO) energy levels of the coloured isomers are between -3.9 and -4.0 eV. Their highest occupied molecular orbital (HOMO) energy levels are found between -5.2 eV and -5.3 eV, allowing the process of regeneration with a sufficiently high driving force using I^-/I_3^- redox couple (-4.95 eV).[27]

2.2.2. DFT calculation

To understand why the molecules **NPI-ThPh** and **NPI-FuPh** never get fully discolored, a DFT study was performed following a methodology described by Brazevic and coworkers.[28] This method consists in the optimization of the geometry and calculation of the energy of the different stable forms occurring during the opening process of the photochromic molecule the energy of the maximum points connecting two minima. Indeed, the transition states were not identified as first saddle points but as the maximum point in energetic relaxed tight scans around the reaction coordinate. Yet for the sake of simplicity, we will name them as "TS". The first stable form is the uncolored closed form noted CF, the second is the Cis-Cis (CC) isomer corresponding to the intermediate opened molecule and the third one is the fully opened form Trans-Cis (TC). The two transition states TS1 and TS2 correspond respectively to the transition between the CF and CC isomers and between the CC and TC isomers.
The results are presented in **Figure *4***. The main differences between the molecules are seen on the calculated energies of the CC isomers and TS2. Indeed, due to their lower resonance energy compared to benzene, the thiophene and furan rings can increase the stability of the quinoid form of the dye and consequently they tend to stabilize the CC isomer and the TS2 transition state without modifying significantly the energy of the TS1 transition state. Once in the CC form (after opening or during closing), the molecule can follow two paths, the first is to pass the TS1 energy barrier and go to the CF isomer and the second is to pass the TS2

energy barrier and go to the TC fully opened isomer. In the case of **NPI**, the two barriers are very similar with a difference of 7 kcal mol^{-1} for the CC-TS1 barrier and 6 kcal mol^{-1} for the CC-TS2 barrier allowing both pathways *i.e.* the opening and the closing of the molecule. However, in the case of **NPI-ThPh** and **NPI-FuPh**, the CC-TS2 barrier is still equal to 6 kcal mol^{-1}, but the CC-TS1 barrier is increased. In the case of **NPI-ThPh** this energetic barrier is equal to 10 kcal mol^{-1} and in the case of **NPI-FuPh** is risen to 13 kcal mol^{-1}. This increased barrier to reach the closed form CF favours the opening of the molecule to the point where it is more favourable for the molecule to stay partially opened.

This explains as well the higher colourability of the thiophene and furan-based photochromic dyes that will generate a higher amount of coloured isomers under illumination compared to **NPI** and the persistence of their coloured form even when the light is off.

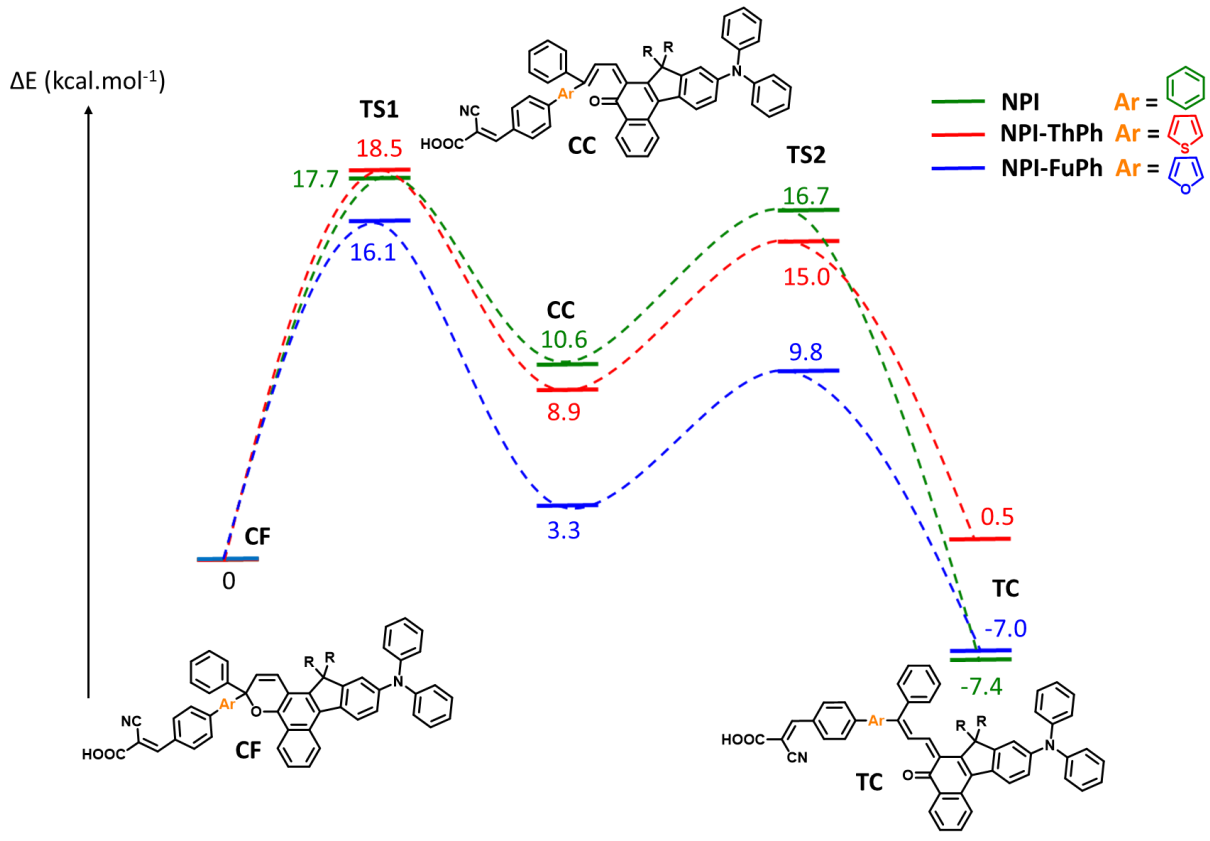

Figure 4. Energies of the different isomers CF, CC, TC of **NPI** (Green), **NPI-ThPh** (Red) and **NPI-FuPh** (Blue) and estimation of the energy of the transition states TS1 and TS2. Energies were normalized compared to the energy of the CF isomer. (Functional: B3LYP, basis set: def2-tzvp)

The formation of the transoid-cis (TC) isomer is the first step towards the generation of more thermally stable open isomers. Indeed, it was demonstrated that trans-cis coloured isomers could upon prolonged irradiation, evolve into the more stable transoid-trans open isomers (TT) responsible for a persistent coloration.

2.3. Dye sensitized solar cells

2.3.1. Evaluation of the performance of the photochromic photosensitizers

The photovoltaic performances of the photochromic photosensitizers were evaluated by fabricating opaque DSSCs. For comparison purposes, the three dyes were tested with the same device configuration under irradiation AM1.5G at 1000 W m^2. TiO_2 mesoporous electrodes were composed of a 13 µm-thick transparent layer covered by a 4 µm-thick scattering layer. We fabricated solar cells using the homemade electrolyte that we developed for the **NPI** dye. In this electrolyte, the *tertio*-butyl pyridine was eliminated to keep an energy offset between the LUMO of the dyes and the conduction band (CB) of the oxide to favour the electron injection.[14]

We recorded the current-voltage characteristics at different time intervals of exposure to light, open-circuit voltage (Voc), fill factor (FF), the short-circuit current density (Jsc), and PCE were determined. For the sensitization, the dyes were used with chenodeoxycholic acid (CDCA) as co-adsorbent. All experimental details for the fabrication of the devices are given in ESI.

During the fabrication of the devices, we noticed that contrarily to **NPI**, the electrodes were coloured right after sensitization in the case of **NPI-ThPh** and **NPI-FuPh**. Indeed, for **NPI-ThPh**, the electrode was light green and for **NPI-FuPh**, the electrode was almost black. In the case of **NPI**, we can observe that the PCE of the cells is constantly increasing between the beginning of the irradiation and the reaching of the PSS alongside the coloration of the cell. **NPI** cells yield a PCE of 3.28 % after 15s under irradiation that goes up to 4.16 % after several minutes when the equilibrium and hence the photo-stationary state is reached. The

IPCE measurements on **NPI**-cells irradiated for 15s and after few minutes, clearly highlights that the increase of Jsc is related to the accumulation of open form isomers that contribute significantly to the generation of current in the visible region. This result is perfectly in line with our previous report. The dyes embedding a thiophene or a furan unit in the chemical structure show a different behaviour under irradiation when compared to **NPI**.

We can see that the PCE of **NPI-ThPh** and **NPI-FuPh** based solar cells is decreasing between 15s and 240s when the PSS is reached. For the three dyes, we observe a drop of the V_{oc} with increasing the irradiation time. This behaviour is common to all the photochromic dyes that we reported so far and we demonstrated that the drop of the V_{oc} in photochromic solar cells is due to a decrease of the recombination resistance (acceleration of the recombinaison kinetics) when switching from the non-coloured form to the coloured isomers.[29]

In the case of **NPI-FuPh**, the PCE after 15s under irradiation and at the PSS is almost the same, which is explained by the fact that the electrode is strongly coloured after sensitization. The photochromic behaviour is not detected in this case in solar cells and the IPCE measurements of **NPI-FuPh**-cells after 15s under irradiation and after a few minutes is almost the same. However, we systematically noticed a slight increase of the J_{sc} under irradiation with **NPI-FuPh**-cells. This effect may be attributed to the remaining closed molecules that are opening or a light soaking effect.[30] To demonstrate that the molecule still behaves as a photochromic dye after grafting on the surface of TiO_2, 2µm-thick transparent electrodes were tainted and UV-visible spectra were recorded before and after exposure to light. This experiment clearly demonstrates that the photochromic process can still happen after the grafting the dye but an additional light soaking effect cannot be ruled out.

The light rise of J_{sc} does not compensate the loss of V_{oc} and consequently the PCE slightly decreases to stabilize at 2.61 % at the PSS. **NPI-FuPh** shows lowest performance compared to the other dyes, due to a lower V_{oc} (around 0.44 V at PSS).

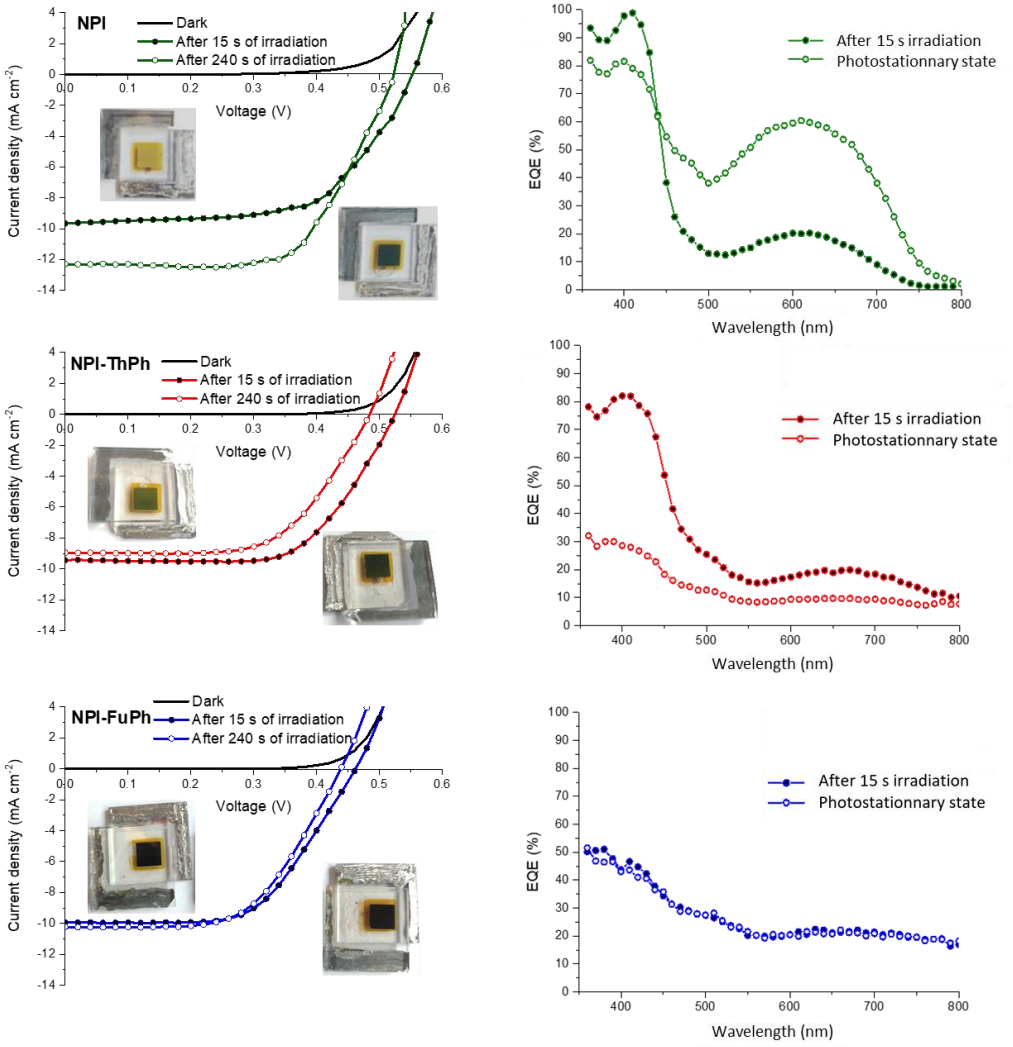

Figure 5. One the left, current–voltage (J, V) curves for **NPI**, **NPI-FuPh** and **NPI-ThPh** in the dark (black line), after a few seconds of irradiation (dashed line) and at the PSS (plain line). On the right, IPCE at the wavelength range of 350 - 800 nm for **NPI**, **NPI-FuPh** and **NPI-ThPh**

Table 2. Photovoltaic parameters of compounds **NPI**, **NPI-FuPh** and **NPI-ThPh**, under irradiation AM1.5G at 1000 W m2; Electrodes: TiO2 mesoporous anatase (13 µm) + scattering layer (4 µm)

Dye	Jsc (mA cm-2)	Voc (V)	FF (%)	PCE (%)
NPI	9.66[a)] 12.29[b)] (12.14 ± 0.11)[c)]	0.552[a)] 0.523[b)] (0.521 ± 0.007)[c)]	61.5[a)] 64.8[b)] (65.4 ± 0.9)[c)]	3.28[a)] 4.16[b)] (4.13 ± 0.02)[c)]
NPI-FuPh	9.94[a)] 10.23[b)] (9.91 ± 0.32)[c)]	0.462[a)] 0.439[b)] (0.441 ± 0.011)[c)]	58.9[a)] 58.4[b)] (58.7 ± 0.6)[c)]	2.71[a)] 2.61[b)] (2.56 ± 0.05)[c)]
NPI-ThPh	9.44[a)] 8.97[b)] (9.38 ± 0.36)[c)]	0.525[a)] 0.484[b)] (0.454 ± 0.026)[c)]	64.6[a)] 61.4[b)] (61.6 ± 0.8)[c)]	3.20[a)] 2.66[b)] (2.62 ± 0.04)[c)]

[a)]: best cell (irradiation time 15s); [b)]: best cell at PSS (irradiation time 240 s) ; [c)]: mean results and deviation calculated on 3 cells at PSS

Obtaining lower V_{oc} values when a furan is inserted close to the anchoring group is not surprising since several groups have reported this phenomenon before with classical dyes. In previous studies, the V_{oc} loss was attributed to an increase of the charge recombination rate[31] or a conduction band downshift of the metal oxide.[32] This will be commented in details in the next section. In the case of **NPI-ThPh**, the loss of PCE is due to a simultaneous loss of V_{oc} and J_{sc} during the coloration of the cells. **NPI-ThPh** solar cells give a PCE of 3.20 % after 15s under irradiation, which goes down to 2.66 % at the PSS despite the fact that the electrode changes colour and become darker. IPCE experiments clearly confirms that the **NPI-ThPh** solar cells are less efficient to convert visible photons into electrons when a larger portion of the molecules are isomerized in the open form. The V_{oc} of the **NPI-ThPh** cells is lower than the one obtained with **NPI** (around 0.45 V versus 0.52V). To understand better the origin of the lower V_{oc} obtained with furan and thiophene based dyes and the photovoltaic behaviour of these photochromic dyes, an impedance spectroscopy study was undertaken. The results are presented in the next section.

2.3.2. Impedance spectroscopy

Despite the introduction of electron-rich groups towards higher absorption properties of the dyes, the performances of the photochromic solar cells fabricated with the new compounds were rather disappointing. A huge V_{oc} loss with irradiation time is observed leading to poorer PCEs at the PSS compared to **NPI**. To shed light on the origin of the V_{oc} loss and the J_{sc} stagnation or decrease, impedance spectroscopy on the photochromic cells was performed following the same method as described in our previous work.[29]

As was already shown, there is no observable band shift between the cells in their "deactivated" state and the cells in their "activated" state (See ESI). **Figure 6** shows the capacitances *versus* the applied voltages in the **NPI**, **NPI-FuPh** and **NPI-ThPh** -based cells. For all the dyes, the variation is exponential in accordance with exponentially distributed traps

in TiO_2.[33] The trends observed in these plots seem to be parallel to each other thus making the systems different. Given the dependence of the photovoltage on the band edge and the redox potential, one possible explanation could be a band edge shift towards more negative values hence explaining why[34,35] the cells with highest V_{oc} are **NPI** devices and the lowest are **NPI-FuPh** ones. Indeed, under operating conditions with reference to **NPI**-based cells, a bandshift of 35 mV and 67 mV was noted in **NPI-ThPh** and **NPI-FuPh** devices, respectively. Analysing the Nyquist plots, we noticed a shrink in the semi-cicle after irradiation. This behaviour is the sign of a reduction of the recombination resistance during the irradiation due to the creation of paths for the iodine to get closer to the titanium dioxide surface and recombine. This behaviour can also be explained by the important reduction of the recombination resistance. Indeed, at the same traps filling, the resistance goes from 2.10^3 Ω for **NPI** cells to 5.10^2 Ω for **NPI-ThPh** and 4.10^1 Ω for **NPI-FuPh**. As **Figure 6a** shows a bandshift between the three dyes studied, a voltage correction is required to ensure that the comparisons are done at the same electron quasi-Fermi level so the electron density in the photoanode under different light intensities is the same.[36–38] This correction allows for comparison leading to **Figure 6b** plot thus comparing the recombination kinetics at similar levels of traps filling. From the Nyquists plots at the corrected voltages (see **Figure 6c**), the recombination resistances at the same electron density decreases from **NPI** to **NPI-ThPh** to **NPI-FuPh**, a similar fashion as their photovoltaic performance in devices. The recombination resistance decreases exponentially as a function of the open-circuit voltage with comparable slopes and the recombination parameter, β, lies in the (0.83-0.86) range, which is in consonance with what is commonly observed in both, photochromic and non-photochromic dyes.[29,34,39–41] In conclusion, from the impedance study it can be stated that the recombination processes in **NPI**-based cells are much slower than for both modificated dyes, and among them, the **NPI-FuTh** cells show a very accelerated recombination and a band shift

towards more negative potentials, both explaining the lower Voc measured with respect to the reference **NPI** dye.

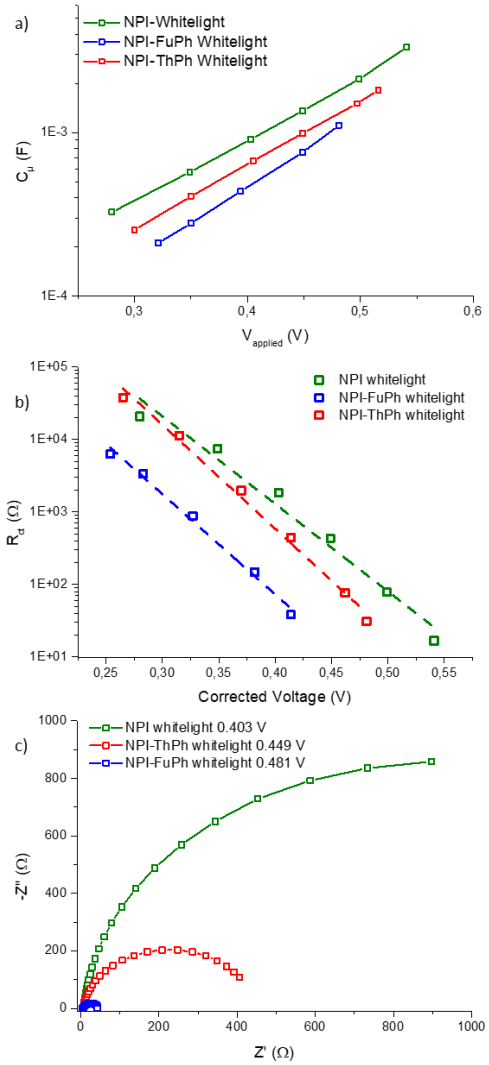

Figure 6. Electrochemical impedance study of **NPI**, **NPI-ThPh**, and **NPI-FuPh** based solar cells a) showing the extracted chemical capacitances (C_μ) after fitting the data to an equivalent circuit, b) the recombination resistances under white illumination at the corrected voltages, and c) the Nyquists plots at the corrected voltages for comparison at similar electron density at the quasi-Fermi level.

The low PCE and spectral response of **NPI-FuTh** and **NPI-ThPh** cells as compared to **NPI** could be a result of either poor electronic injection or poor regeneration. However, these possibilities were ruled out given the comparable HOMO and LUMO locations as determined experimentally (see ESI). However, the impedance study also suggest that the decrease in the

overall photovoltaic performance (with a decrease in the Jsc as well) is due to increased recombination. This finding is in good agreement with previous reports where thiophene or furan spacers are often implicated in the increase of recombination by binding I_2 near the semiconductor surface.[42–45]

Finally, we modelled the SOMO level of the oxidized dyes after electron injection by DFT. The SOMO orbitals of **NPI-ThPh** and **NPI-FuPh** appear to extend towards the cyano-acrylic anchoring function unlike in **NPI** (see ESI). This suggests that, other than the accelerated recombination occurring at the TiO_2/electrolyte interface of **NPI-FuPh** and **NPI-ThPh** based devices, the TiO_2/oxidized dye recombination could be favoured with these dyes.

3. Conclusion

Two photochromic dyes **NPI-ThPh** and **NPI-FuPh** based on diaryl-naphthopyran core were synthesised, fully characterised and tested in dye solar cells with the goal to build structure properties relationships for this new class of multifunctional dyes. The molecules are analogues to **NPI** dye (our reference dye) and they only vary by the nature of the spacer, a thiophene or a furan, connecting the photochromic unit and a phenyl-cyano-acrylic acid unit used as the anchoring function. We found that the introduction of a thiophene or a furan ring in the chemical structure leads to an improvement of absorption properties of the molecules when studied in solution. The new photochromic dyes demonstrate a higher colorability compared to **NPI**. Notably, the absorption spectrum of the coloured species is bathochromically shifted and the absorption band edge of the molecules reaches the NIR region. Unfortunately, the reversibility of the photochromic process is negatively impacted by the presence of the thiophene or the furan near the photochromic unit. The thermal decoloration kinetic is slowed down and a remaining coloration is observed in solution. A DFT study showed that these phenomena originate from the stabilisation of the CC isomer that is involved in the interconversion mechanism between the colored and non-colored isomers. Despite better absorption in the visible range of their colored isomers, the two new dyes show lower photochromic and photovoltaic properties in devices compared to **NPI**. Thanks to impedance spectroscopy experiments, we showed that the recombination resistance is strongly reduced in **NPI-ThPh** and **NPI-FuPh** cells as well as the negative bandshifts, which explain the lower V_{oc} and PCE

obtained with these dyes in comparison with our reference dye. We highlight here that design rules established to improve the performances of classical organic photosensitizers in DSSC cannot be directly applied to photochromic dyes. Our study contributes to understand better the relationships between photochromic and photovoltaic properties within this novel class of multifunctional dyes. The introduction of a thiophene or furan unit close to the naphthopyran ring is found beneficial to the absorption properties of the molecules but it changes the photochromic behaviour drastically. An alternative strategy could be to introduce this type of units close to the anchoring function, with a spacer to separate it from the naphthopyran unit. This strategy is currently under exploration. We believe, that the structure properties relationships that we established through this work will be useful for future developments of photochromic photosensitizers.

Supporting Information

Supporting Information is available from the Wiley Online Library or from the author.

Acknowledgements

R. D. acknowledges ANR for funding through the ODYCE project (grant agreement number ANR-14-OHRI-0003-01). J. L. acknowledges CEA for funding through a CFR PhD grant. R. D. acknowledges the European Research Council (ERC) for funding. This work was funded under the European Union's Horizon 2020 research and innovation programme (grant agreement number 832606; project PISCO). J.A.A acknowledges the Ministerio de Ciencia e Innovación of Spain, Agencia Estatal de Investigación (AEI) and EU (FEDER) under grants PID2019-110430GB-C22 and PCI2019-111839-2 (SCALEUP) and Junta de Andalucia under grant SOLARFORCE (UPO-1259175). A.J.R. thanks the Spanish Ministry of Education, Culture and Sports for its supports via a PhD grant (FPU2017-03684).

Received: ((will be filled in by the editorial staff))
Revised: ((will be filled in by the editorial staff))
Published online: ((will be filled in by the editorial staff))

The data that support the findings of this study are available from the corresponding author upon reasonable request and in the supporting information.

References

[1] S. G. Yalew, M. T. H. van Vliet, D. E. H. J. Gernaat, F. Ludwig, A. Miara, C. Park, E. Byers, E. De Cian, F. Piontek, G. Iyer, I. Mouratiadou, J. Glynn, M. Hejazi, O. Dessens, P. Rochedo, R. Pietzcker, R. Schaeffer, S. Fujimori, S. Dasgupta, S. Mima, S. R. S. da Silva, V. Chaturvedi, R. Vautard, D. P. van Vuuren, *Nat. Energy* **2020**, *5*, 794–802.
[2] Y. Cao, Y. Liu, S. M. Zakeeruddin, A. Hagfeldt, M. Grätzel, *Joule* **2018**, *2*, 1108–1117.
[3] D. Zhang, M. Stojanovic, Y. Ren, Y. Cao, F. T. Eickemeyer, E. Socie, N. Vlachopoulos, J.-E. Moser, S. M. Zakeeruddin, A. Hagfeldt, M. Grätzel, *Nat. Commun.* **2021**, *12*, 1777.
[4] M. Godfroy, J. Liotier, V. M. Mwalukuku, D. Joly, Q. Huaulmé, L. Cabau, C. Aumaitre, Y. Kervella, S. Narbey, F. Oswald, E. Palomares, C. A. G. Flores, G. Oskam, R. Demadrille, *Sustain. Energy Fuels* **2021**, *5*, 144–153.
[5] H. Michaels, M. Rinderle, R. Freitag, I. Benesperi, T. Edvinsson, R. Socher, A. Gagliardi, M. Freitag, *Chem. Sci.* **2020**, *11*, 2895–2906.
[6] R. Haridas, J. Velore, S. C. Pradhan, A. Vindhyasarumi, K. Yoosaf, S. Soman, K. N. N. Unni, A. Ajayaghosh, *Mater. Adv.* **2021**, DOI 10.1039/D1MA00829C.
[7] H. Zheng, D. Li, C. Ran, Q. Zhong, L. Song, Y. Chen, P. Müller-Buschbaum, W. Huang, *Sol. RRL* **2021**, *5*, 2100042.
[8] D. Joly, L. Pellejà, S. Narbey, F. Oswald, T. Meyer, Y. Kervella, P. Maldivi, J. N. Clifford, E. Palomares, R. Demadrille, *Energy Environ. Sci.* **2015**, *8*, 2010–2018.
[9] F. Sauvage, *Adv. Chem.* **2014**, *2014*, e939525.
[10] S. Yoon, S. Tak, J. Kim, Y. Jun, K. Kang, J. Park, *Build. Environ.* **2011**, *46*, 1899–1904.
[11] G. Maddala, M. Ambapuram, V. Tankasala, R. Mitty, *ACS Appl. Energy Mater.* **2021**, *4*, 11225–11233.
[12] M. Pagliaro, G. Palmisano, R. Ciriminna, V. Loddo, *Energy Environ. Sci.* **2009**, *2*, 838–844.
[13] K. Zhang, C. Qin, X. Yang, A. Islam, S. Zhang, H. Chen, L. Han, *Adv. Energy Mater.* **2014**, *4*, 1301966.
[14] Q. Huaulmé, V. M. Mwalukuku, D. Joly, J. Liotier, Y. Kervella, P. Maldivi, S. Narbey, F. Oswald, A. J. Riquelme, J. A. Anta, R. Demadrille, *Nat. Energy* **2020**, *5*, 468–477.
[15] F. Ortica, P. Smimmo, G. Favaro, U. Mazzucato, S. Delbaere, D. Venec, G. Vermeersch, M. Frigoli, C. Moustrou, A. Samat, *Photochem. Photobiol. Sci.* **2004**, *3*, 878–885.
[16] Y. K. Eom, J. Y. Hong, J. Kim, H. K. Kim, *Dyes Pigments* **2017**, *136*, 496–504.
[17] L. Cabau, C. V. Kumar, A. Moncho, J. N. Clifford, N. López, E. Palomares, *Energy Environ. Sci.* **2015**, *8*, 1368–1375.
[18] J. Yang, F. Guo, J. Hua, X. Li, W. Wu, Y. Qu, H. Tian, *J. Mater. Chem.* **2012**, *22*, 24356–24365.
[19] X. Zhang, L. Chen, X. Li, J. Mao, W. Wu, H. Ågren, J. Hua, *J. Mater. Chem. C* **2014**, *2*, 4063–4072.
[20] T. Hua, K. Zhang, Z.-S. Huang, L. Wang, H. Tang, H. Meier, D. Cao, *J. Mater. Chem. C* **2019**, *7*, 10379–10388.
[21] P. Allegrini, N. Nodari, L. Crisci, V. Malatesta, *New Photochromic Naphto(2,1-b)Pyrans and Method for Their Preparation.*, **1994**, EP0629620A1.
[22] A. Oster, T. Klein, C. Henn, R. Werth, S. Marchais-Oberwinkler, M. Frotscher, R. W. Hartmann, *ChemMedChem* **2011**, *6*, 476–487.
[23] F. L. Zheng, S. R. Ban, X. E. Feng, C. X. Zhao, W. Lin, Q. S. Li, *Molecules* **2011**, *16*, 4897–4911.
[24] B.-G. Kim, K. Chung, J. Kim, *Chem. – Eur. J.* **2013**, *19*, 5220–5230.
[25] M. Cariello, S. M. Abdalhadi, P. Yadav, J.-D. Decoppet, S. M. Zakeeruddin, M. Grätzel, A. Hagfeldt, G. Cooke, *Dalton Trans.* **2018**, *47*, 6549–6556.

[26] H. Cao, P. A. Rupar, *Chem. – Eur. J.* **2017**, *23*, 14670–14675.
[27] T. W. Hamann, R. A. Jensen, A. B. F. Martinson, H. V. Ryswyk, J. T. Hupp, *Energy Environ. Sci.* **2008**, *1*, 66–78.
[28] S. Brazevic, S. Nizinski, R. Szabla, M. F. Rode, G. Burdzinski, *Phys. Chem. Chem. Phys.* **2019**, *21*, 11861–11870.
[29] A. J. Riquelme, V. M. Mwalukuku, P. Sánchez-Fernández, J. Liotier, R. Escalante, G. Oskam, R. Demadrille, J. A. Anta, *ACS Appl. Energy Mater.* **2021**, *4*, 8941–8952.
[30] A. Listorti, C. Creager, P. Sommeling, J. Kroon, E. Palomares, A. Fornelli, B. Breen, P. R. F. Barnes, J. R. Durrant, C. Law, B. O'Regan, *Energy Environ. Sci.* **2011**, *4*, 3494–3501.
[31] H. Jia, X. Ju, M. Zhang, Z. Ju, H. Zheng, *Phys. Chem. Chem. Phys.* **2015**, *17*, 16334–16340.
[32] S. Qu, B. Wang, F. Guo, J. Li, W. Wu, C. Kong, Y. Long, J. Hua, *Dyes Pigments* **2012**, *92*, 1384–1393.
[33] J. A. Anta, J. Idígoras, E. Guillén, J. Villanueva-Cab, H. J. Mandujano-Ramírez, G. Oskam, L. Pellejà, E. Palomares, *Phys. Chem. Chem. Phys.* **2012**, *14*, 10285–10299.
[34] E. Guillén, L. M. Peter, J. A. Anta, *J. Phys. Chem. C* **2011**, *115*, 22622–22632.
[35] S. R. Raga, E. M. Barea, F. Fabregat-Santiago, *J. Phys. Chem. Lett.* **2012**, *3*, 1629–1634.
[36] F. Fabregat-Santiago, G. Garcia-Belmonte, I. Mora-Seró, J. Bisquert, *Phys. Chem. Chem. Phys.* **2011**, *13*, 9083–9118.
[37] L. M. Peter, *J. Phys. Chem. C* **2007**, *111*, 6601–6612.
[38] D. Pourjafari, D. Reyes-Coronado, A. Vega-Poot, R. Escalante, D. Kirkconnell-Reyes, R. García-Rodríguez, J. A. Anta, G. Oskam, *J. Phys. Chem. C* **2018**, *122*, 14277–14288.
[39] J. Bisquert, A. Zaban, P. Salvador, *J. Phys. Chem. B* **2002**, *106*, 8774–8782.
[40] J. Bisquert, I. Mora-Seró, *J. Phys. Chem. Lett.* **2010**, *1*, 450–456.
[41] J. Bisquert, *Phys. Chem. Chem. Phys.* **2003**, *5*, 5360–5364.
[42] A. Baumann, H. Cheema, M. A. Sabuj, L. E. McNamara, Y. Zhang, A. Peddapuram, S. T. Nguyen, D. L. Watkins, N. I. Hammer, N. Rai, J. H. Delcamp, *Phys. Chem. Chem. Phys.* **2018**, *20*, 17859–17870.
[43] S. Aghazada, P. Gao, A. Yella, G. Marotta, T. Moehl, J. Teuscher, J.-E. Moser, F. De Angelis, M. Grätzel, M. K. Nazeeruddin, *Inorg. Chem.* **2016**, *55*, 6653–6659.
[44] A. F. Buene, D. M. Almenningen, *J. Mater. Chem. C* **2021**, *9*, 11974–11994.
[45] M. Zhang, J. Liu, Y. Wang, D. Zhou, P. Wang, *Chem. Sci.* **2011**, *2*, 1401–1406.

Johan Liotier, Valid Mwatati Mwalukuku, Antonio J. Riquelme, Juan A. Anta, Pascale Maldivi and Renaud Demadrille*

Photochromic naphthopyran dyes incorporating a benzene, thiophene or furan spacer: effect on photochromic, optoelectronic and photovoltaic properties in dye-sensitized solar cells.

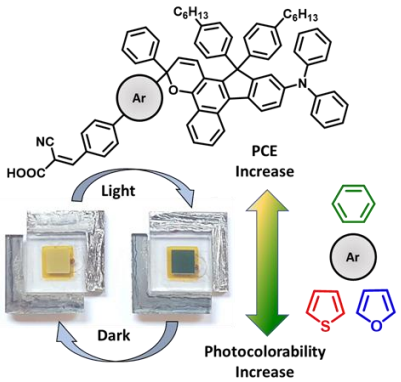

We report two new photochromic photosensitizers for use in dye-sensized solar cells. Thanks to UV-Vis spectroscopy, DFT calculations, electrical and impedance spectroscopy characterizations of the solar cells, we unravel important relationships between structure, photochromic and photovoltaic properties within this novel class of multifunctional dyes.

Supporting Information

Photochromic naphthopyran dyes incorporating a benzene, thiophene or furan spacer: effect on photochromic, optoelectronic and photovoltaic properties in dye-sensitized solar cells.

*Johan Liotier, Valid Mwatati Mwalukuku, Antonio J. Riquelme, Juan A. Anta, Pascale Maldivi and Renaud Demadrille**

I) Synthesis

Compound **10** was synthesised according to literature. [1]

General procedure for chromenisation reaction:

To a solution of compound 1.7 (1.00 eq) in anhydrous DCE are successively added propargilyc alcohols, PPTS (10 mol%) and trimethylorthoformate (3.0 eq). The mixture is stirred at 70°C for 72 hours. A 6M hydrochloric acid solution in water is then added and the reaction mixture is stirred at 60 °C during 4 hours. Once cooled down to room temperature, the reaction mixture is poured on water and DCM is added. The layers are separated. The organic layer is washed with water, dried over Na2SO4, filtered off and concentrated under vacuum. The resulting oil is purified by column chromatography (Hexane/DCM 8/2 to Hexane/DCM 6/4).

General procedure for Knoevenagel reaction:

The aldhehyde (1.00 eq) is dissolved in Toluene. Cyanoacetic acid (6.00 eq) and ammonium acetate (16.0 eq) is then added and the reaction mixture is stirred at 100 °C for 16 h. Water and EtOAc are added to the mixture, which is further stirred at room temperature for 10 minutes. The layers are separated and the aqueous layer is extracted once with EtOAc. The combined organic layer is dried over Na2SO4, filtered off and concentrated under vacuum. The resulting residue is purified by column chromatography (silica gel, neat DCM to DCM/MeOH: 90/10).

Compound **2**:

To a solution of Bromo-furfural (1.00 g, 5.71 mmol, 1.00 eq) in THF (50 mL) is added a solution of phenylmagnesium bromide (3 M in THF, 3.81 mL, 11.43 mmol, 2.00 eq). The solution in stirred to RT for 2 hours. The solvent in then evaporated. The resulting alcohol was not purified and solubilized in DCM (50 mL). Manganese dioxide (7.45 g, 85.72 mmol,

15 eq) was then added and the reaction mixture was stirred for 16 hours. The mixture is extracted three times with dichloromethane. The organic layers are combined washed with water, dried over Na2SO4, filtered off and concentrated under vacuum. The crude product is purified by column chromatography (Silica gel, Hexane/DCM: 90/10 to 70/30) to afford compound **2** as a brown solid (0.802 g, 3.27 mmol, 57 %). **^{1}H-NMR (CDCl3, 400 MHz) δ (ppm):** 7.92 – 7.79 (m, 1H), 7.51 (t, J = 7.4 Hz, 1H), 7.40 (dd, J = 11.5, 4.1 Hz, 1H), 7.08 (d, J = 3.5 Hz, 1H), 6.47 (d, J = 3.1 Hz, 1H). **^{13}C-NMR (CDCl3, 100 MHz) δ (ppm):** 180.86 (s), 153.82 (s), 136.53 (s), 132.80 (s), 129.14 (s), 128.53 (s), 122.55 (s), 114.38 (s). **MS (ESI-TOF):** calcd. for C11H7O2Br, 251.0 ; found 251.1.

Compound **3**:

Benzoyl chloride (1.4 mL, 12 mmol, 1.00 eq) and 2-bromothiophene (1.16 mL, 12 mmol, 1.00 eq) are dissolved in chloroform (60 mL) and cooled to 0 °C. Aluminium chloride (1.96 g, 14.6 mmol, 1.2 eq) is then slowly added by portion. The reaction mixture is then stirred at 0 °C during 45 minutes then 30 minutes at room temperature. A solution of HCl 2M (30 mL) is then slowly added to stop the reaction. The mixture is extracted three times with dichloromethane. The organic layers are combined washed with water, dried over Na2SO4, filtered off and concentrated under vacuum. The crude product is purified by column chromatography (Silica gel, Hexane/DCM: 80/20 to 40/60) to afford compound **3** as a brown solid (1.55 g, 5.8 mmol, 48%). **^{1}H-NMR (CDCl3, 400 MHz) δ (ppm):** 7.87-7.83 (m, 2H), 7.66-7.60 (m, 1H), 7.56-7.49 (m, 2H), 7.41 (d, J = 4.0 Hz, 1H), 7.16 (d, J = 4.0 Hz, 1H). **^{13}C-NMR (CDCl3, 100 MHz) δ (ppm):** 186.99, 145.11, 137.39, 134.97, 132.52, 131.15, 129.05, 128.56, 123.20. **MS (ESI-TOF):** calcd. for C11H7OSBr, 266.9 ; found 267.1.

Compound **4**:

4-bromobenzophenone (1.15 g, 4.40 mmol, 1.00 eq) and 2-(4-(5,5-dimethyl-1,3-dioxan-2-yl)phenyl)-4,4,5,5-tetramethyl-1,3,2-dioxaborolane (1.54 g, 4.84 mmol, 1.10 eq) are dissolved in dioxane (15 mL). The mixture is degassed by argon bubbling during 30 minutes.

Pd(dppf)Cl2 (70 mg, 0.096 mmol, 2 mol%) is then added followed by 1M AcOK solution in water (13.21 mL, 13.21 mmol, 3 eq). The reaction mixture is then heated to 70 °C and stirred 18 hours. Water and EtOAc are added to the mixture, which is further stirred at room temperature for 10 minutes. The layers are separated and the aqueous layer is extracted once with EtOAc. The combined organic layer is dried over Na2SO4, filtered off and concentrated under vacuum. The crude product is precipitated in PE to afford compound **4** as a brown solid (1.44 g, 3.87 mmol, 88%). **^{1}H-NMR (CDCl3, 400 MHz) δ (ppm):** 7.95 (d, J = 3.8 Hz, 1H), 7.90 (d, J = 4.0 Hz, 1H), 7.76-7.69 (m, 3H), 7.60 (d, J = 8.2 Hz, 2H), 7.40 (d, J = 4.0 Hz, 1H), 7.24-7.20 (m, 1H), 3.81 (d, J = 11.0 Hz, 2H), 3.69 (d, J = 11.0 Hz, 2H), 1.33 (s, 3H), 0.84 (s, 3H). **^{13}C-NMR (CDCl3, 100 MHz) δ (ppm):** 178.45, 152.17, 142.83, 141.73, 139.42, 134.26, 133.67, 133.35, 132.93, 128.00, 127.04, 126.23, 124.14, 101.06, 77.67, 30.27, 23.07, 21.89. **MS (ESI-TOF):** calcd. for C27H26O3, 373.2 ; found 373.3.

Compound **5**:

Compound **2** (1.00 g, 3.74 mmol, 1.00 eq) and 2-(4-(5,5-dimethyl-1,3-dioxan-2-yl)phenyl)-4,4,5,5-tetramethyl-1,3,2-dioxaborolane (1.30 g, 4.09 mmol, 1.10 eq) are dissolved in dioxane (10 mL). The mixture is degassed by argon bubbling during 30 minutes. Pd(dppf)Cl2 (59.9 mg, 81.8 µmol, 2 mol%) is then added followed by 1M AcOK solution in water (11.22 mL, 11.22 mmol, 3 eq). The reaction mixture is then heated to 70 °C and stirred 18 hours. Water and EtOAc are added to the mixture, which is further stirred at room temperature for 10 minutes. The layers are separated and the aqueous layer is extracted once with EtOAc. The combined organic layer is dried over Na2SO4, filtered off and concentrated under vacuum. The crude product is precipitated in PE to afford compound **5** as a brown solid (953 mg, 2.52 mmol, 67%). **^{1}H-NMR (CDCl3, 400 MHz) δ (ppm):** 7.90 (d, J = 7.7 Hz, 2H), 7.73 (d, J = 7.7 Hz, 2H), 7.62 (dd, J = 15.3, 5.7 Hz, 4H), 7.54 (t, J = 7.4 Hz, 2H), 7.39 (d, J = 3.9 Hz, 1H), 3.82 (d, J = 10.8 Hz, 2H), 3.70 (d, J = 10.8 Hz, 2H), 1.33 (s, 3H), 0.84 (s, 3H). **^{13}C-NMR (CDCl3, 100 MHz) δ (ppm):** 180.76, 135.93, 132.22, 129.12, 128.46, 127.19, 127.01,

126.52, 126.30, 124.10, 101.06, 71.04, 32.64, 23.05, 21.90. **MS (ESI-TOF):** calcd. for C25H24O3S, 405.2 ; found 405.2.

Compound **6**:

Compound **3** (400 g, 70.7 mmol, 1.00 eq) and 2-(4-(5,5-dimethyl-1,3-dioxan-2-yl)phenyl)-4,4,5,5-tetramethyl-1,3,2-dioxaborolane (608.4 mg, 1.91 mmol, 1.10 eq) are dissolved in dioxane (5 mL). The mixture is degassed by argon bubbling during 30 minutes. Pd(dppf)Cl2 (23.31 mg, 31.86 µmol, 2 mol%) is then added followed by 3M AcOK solution in water (1.59 mL, 4.78 mmol, 3 eq). The reaction mixture is then heated to 70 °C and stirred 18 hours. Water and EtOAc are added to the mixture, which is further stirred at room temperature for 10 minutes. The layers are separated and the aqueous layer is extracted once with EtOAc. The combined organic layer is dried over Na2SO4, filtered off and concentrated under vacuum. The crude product is precipitated in PE to afford compound **6** as a brown solid (375 mg, 1.59 mmol, 65%). **^{1}H-NMR (CDCl3, 400 MHz) δ (ppm):** 8.03 (dd, J = 5.2, 3.2 Hz, 3H), 7.86 (d, J = 8.3 Hz, 2H), 7.68 – 7.50 (m, 8H), 7.34 (dd, J = 6.7, 3.7 Hz, 1H), 7.08 (d, J = 3.7 Hz, 1H), 6.88 (d, J = 3.7 Hz, 1H), 5.45 (s, 1H), 3.82 (d, J = 11.1 Hz, 3H), 3.70 (d, J = 11.0 Hz, 3H), 1.33 (s, 4H), 0.84 (s, 3H). **^{13}C-NMR (CDCl3, 100 MHz) δ (ppm):** 139.52 (s), 137.62 (s), 132.81 (s), 132.40 (s), 129.69 (s), 129.28 (s), 128.56 (s), 128.43 (s), 127.16 (s), 126.83 (s), 126.54 (s), 125.08 (s), 122.88 (s), 122.32 (s), 110.14 (s), 107.75 (s), 101.47 (s), 101.19 (s), 30.30 (s), 23.06 (s), 21.90 (s). **MS (ESI-TOF):** calcd. for C23H22O4, 363.2 ; found 363.3.

Compound **7**:

Trimethylsilylacetylene (0.08 mL, 5.41 mmol, 1.40 eq) is dissolved in THF (10 mL). The reaction mixture is cooled to 0°C and 2.5 M nBuLi solution in hexane (2.17 mL, 5.41 mmol, 1.40 eq) is added dropwise. The reaction mixture is further stirred at this temperature for 30 min. Compound **4** (1.44 g, 3.87 mmol, 1.00 eq) is then added in one portion as a solid and the reaction mixture is allowed to warm up to room temperature and stirred 18 hours. A solution of sodium hydroxide (0.928 g, 26.20 mmol, 6.00 eq) in methanol (1 mL) is added and the

reaction mixture is further stirred for 5 hours. Water (10 mL) is added to stop the reaction. The mixture is extracted three times with ethyl acetate. The organic layers are combined, washed with water dried over Na2SO4, filtered off and concentrated under vacuum. The crude product is precipitated in PE to afford Compound **7** as a brown solid (1.54 g, 3.87 mmol, 100%). **^{1}H-NMR (CDCl3, 400 MHz) δ (ppm):** 7.71 – 7.66 (m, 3H), 7.59 (s, 3H), 7.58 – 7.55 (m, 2H), 7.41 – 7.35 (m, 2H), 7.34 – 7.29 (m, 1H), 5.46 (s, 1H), 3.81 (d, J = 11.2 Hz, 2H), 3.69 (d, J = 10.8 Hz, 2H), 2.93 (s, 1H), 2.88 (s, 1H), 1.33 (s, 3H), 0.84 (s, 3H). **^{13}C-NMR (CDCl3, 100 MHz) δ (ppm):** 128.38, 127.96, 127.13, 127.09, 126.59, 126.40, 125.98, 102.15, 77.70, 76.41, 75.62, 30.37, 23.06, 21.90. **MS (ESI-TOF):** calcd. for C27H26O3, 399.2 ; found 399.2.

Compound **8**:

Trimethylsilylacetylene (0.04 mL, 2.85 mmol, 1.20 eq) is dissolved in THF (10 mL). The reaction mixture is cooled to 0°C and 2.5 M nBuLi solution in hexane (1.15 mL, 2.88 mmol, 1.20 eq) is added dropwise. The reaction mixture is further stirred at this temperature for 30 min. Compound **5** (900 mg, 2.38 mmol, 1.00 eq) is then added in one portion as a solid and the reaction mixture is allowed to warm up to room temperature and stirred 18 hours. A solution of sodium hydroxide (0.35 g, 8.75 mmol, 3.68 eq) in methanol (3 mL) is added and the reaction mixture is further stirred for 5 hours. Water (10 mL) is added to stop the reaction. The mixture is extracted three times with ethyl acetate. The organic layers are combined, washed with water dried over Na2SO4, filtered off and concentrated under vacuum. The crude product is precipitated in PE to afford Compound **8** as a brown solid (760 g, 1.88 mmol, 79%). **^{1}H-NMR (CDCl3, 400 MHz) δ (ppm):** 7.75 (dt, J = 8.1, 4.4 Hz, 1H), 7.60 (d, J = 0.9 Hz, 1 Hz), 7.58-7.54 (m, 2H), 7.50 (d, J = 8.3 Hz, 2H), 7.45-7.33 (m, 3H), 7.13 (d, J = 3.8 Hz, 1H), 7.07 (d, J = 3.8 Hz, 1H), 3.80 (d, J = 11.2 Hz, 2H), 3.68 (d, J = 9.8 Hz, 2H), 3.10 (s, 1.2 Hz, 1H), 2.93 (s, 1H), 1.32 (s, 3H), 0.83 (s, 3H). **^{13}C-NMR (CDCl3, 100 MHz) δ (ppm):** 148.84, 144.80, 143.40, 137.88, 134.64, 128.38, 128.34, 127.17, 126.70, 126.54, 126.44,

125.72, 125.66, 122.61, 101.51, 101.38, 85.55, 77.68, 75.09, 71.79, 30.25, 23.06, 21.89. **MS (ESI-TOF):** calcd. for C23H22O3S, 379.1 ; found 379.3.

Compound **9**:

Trimethylsilylacetylene (0.11 mL, 0.77 mmol, 1.20 eq) is dissolved in THF (5 mL). The reaction mixture is cooled to 0°C and 2.5 M nBuLi solution in hexane (0.3 mL, 0.77 mmol, 1.20 eq) is added dropwise. The reaction mixture is further stirred at this temperature for 30 min. Compound **6** (200 mg, 0.55 mmol, 1.00 eq) is then added in one portion as a solid and the reaction mixture is allowed to warm up to room temperature and stirred 18 hours. A solution of TBAF (1M) in THF (1.10 mL, 1.10 mmol, 2 eq) is added and the reaction mixture is further stirred for 30 minutes. Water (10 mL) is added to stop the reaction. The mixture is extracted three times with ethyl acetate. The organic layers are combined, washed with water dried over Na2SO4, filtered off and concentrated u/nder vacuum. The crude product is purified by column chromatography (silica gel, Hex/DCM: 80/20 - 60/40) afford Compound **9** as a brown solid (150 mg, 0.386 mmol, 70 %). **^{1}H-NMR (CDCl3, 400 MHz) δ (ppm):** 7.77 – 7.72 (m, 2H), 7.67 – 7.62 (m, 2H), 7.53 – 7.48 (m, 2H), 7.45 – 7.34 (m, 3H), 6.59 (d, J = 3.4 Hz, 1H), 6.34 (d, J = 3.4 Hz, 1H), 5.40 (s, 1H), 3.79 (dd, J = 10.0, 1.2 Hz, 2H), 3.67 (d, J = 10.5 Hz, 2H), 2.87 (s, 1H), 2.19 (s, 1H), 1.32 (s, 3H), 0.82 (s, 3H). **^{13}C-NMR (CDCl3, 100 MHz) δ (ppm):** 154.59, 154.34, 141.10, 137.85, 130.89, 128.47, 128.29, 126.51, 126.20, 123.83, 110.17, 105.86, 101.44, 84.06, 74.92, 30.26, 23.06, 21.91. **MS (ESI-TOF):** calcd. for C25H23O3 (Compound **9** without the OH of the propargylic alcohol), 371.2 ; found 371.3.

Compound **11**:

The general chromenisation procedure 1 is followed with compound **10** (450 mg, 0.62 mmol, 1.00 eq), DCE (20 mL), compound **7** (373.59 mg, 0.94 mmol, 1.60 eq), PPTS (52.3 mg, 0.21 mmol, 10 mol%), trimethylorthoformate (0.2 mL, 1.87 mmol, 3 eq) and HCl 6M (20mL) to afford compound **11** as a green solid (180 mg, 0.20 mmol, 26 %). **^{1}H RMN (CD2Cl2, 400MHz) δ (ppm):** 10.01 (s, 1H), 8.60 (d, 1H, 3J = 8.4 Hz), 8.48 (dd, 1H, J = 8.4 Hz, J = 1.1

Hz), 8.02 (d, 1H, 3J = 8.6 Hz), 7.92 (d, 2H, 3J = 8.4 Hz), 7.67 (d, 2H, 3J = 8.4 Hz), 7.40-7.61 (m, 9H), 7.13-7.28 (m, 13H), 6.93-7.03 (m, 11H), 6.74 (d, 1H, J = 9.8 Hz), 5.90 (d, 1H, J = 9.8 Hz), 2.59 (m, 4H), 1.59 (m, 4H), 1.30 (m, 12H), 0.85 (t, 6H). **^{13}C RMN (CD2Cl2, 100MHz) δ (ppm):** 191.6, 146.4, 141.5, 141.5, 139.6, 139.5, 138.8, 135.4, 130.0, 129.6, 129.1, 129.0, 128.8, 128d.8, 128.1, 128.0, 127.9, 127.6, 127.5, 127.3, 127.0, 126.8, 125.3, 124.2, 124.1, 124.1, 124.0, 123.1, 122.8, 122.7, 120.5, 82.0, 64.6, 35.4, 31.7, 31.5, 29.1, 22.6, 13.8.

Compound **12**:

The general chromenisation procedure 1 is followed with compound **10** (200 mg, 0.28 mmol, 1.00 eq), DCE (20 mL), compound **8** (183 mg, 0.45 mmol, 1.60 eq), PPTS (7.00 mg, 0.028 mmol, 10 mol%), trimethylorthoformate (0.86 mL, 0.83 mmol, 3 eq) and HCl 6M (20mL) to afford compound **12** as a green solid (200 mg, 0.20 mmol, 71 %). **^{1}H RMN (CDCl3, 400MHz) δ (ppm):** 9.98 (s, 1H), 8.63 (d, J = 8.3 Hz, 1H), 8.51 (dd, J = 8.4, 1.2 Hz, 1H), 8.04 (d, J = 8.6 Hz, 1H), 7.86-7.80 (m, 2H), 7.66-7.53 (m, 6H), 7.41-7.25 (m, 5H), 7.25-7.14 (m, 9H), 7.10 (d, J = 3.8 Hz, 1H), 7.08-6.96 (m, 12H), 6.77 (d, J = 9.8 Hz, 1H), 6.66 (d, J = 3.8 Hz, 1H), 5.88 (d, J = 9.8 Hz, 1H), 2.68-2.55 (m, 4H), 1.73-1.58 (m, 4H), 1.45-1.24 (m, 12H), 0.97-0.85 (m, 6H). **^{13}C RMN (CDCl3, 100MHz) δ (ppm):** 191.38, 156.66, 150.32, 147.54, 147.34, 146.33, 145.80, 143.61, 143.56, 141.31, 141.18, 139.99, 139.87, 139.38, 135.28, 135.06, 130.30, 129.15, 129.07, 128.85, 128.21, 128.09, 128.06, 127.90, 126.29, 126.17, 125.77, 124.08, 123.99, 122.63, 120.74, 114.85, 79.83, 64.65, 35.60, 35.54, 31.80, 31.75, 31.60, 31.55, 31.41, 29.19, 29.13, 22.66, 22.62, 14.12, 14.10. **MS (ESI-TOF):** calcd. for C73H65O2S, 1020.5 ; found 1020.7.

Compound **13**:

The general chromenisation procedure 1 is followed with compound **10** (100 mg, 0.14 mmol, 1.00 eq), DCE (10 mL), compound **9** (54 mg, 0.14 mmol, 1.00 eq), PPTS (3.50 mg, 0.014 mmol, 10 mol%), trimethylorthoformate (0.27 mL, 0.42 mmol, 3 eq) and HCl 6M (5 mL),

accept that the reaction time was reduced to 16 hours, to afford compound **13** as a green solid (50 mg, 49.8 µmol, 36 %). **^{1}H RMN (CDCl3, 400MHz) δ (ppm):** 9.55 (s, J = 4.4 Hz, 1H), 8.74 – 8.68 (m, 1H), 8.63 – 8.54 (m, 1H), 7.93 – 7.87 (m, 1H), 7.64 – 7.57 (m, 2H), 7.45 – 7.33 (m, 7H), 7.29 – 7.24 (m, 2H), 7.14 – 6.91 (m, 17H), 6.89 – 6.80 (m, 3H), 6.20 (d, J = 3.4 Hz, 1H), 6.12 (d, J = 3.4 Hz, 1H), 5.73 – 5.69 (m, 1H), 2.55 – 2.42 (m, 4H), 1.60 – 1.46 (m, 4H), 1.43 – 1.15 (m, 16H), 0.96 – 0.81 (m, 6H). **^{13}C-NMR (CDCl3, 100 MHz) δ (ppm):** 190.08, 157.02, 155.54, 153.42, 147.97, 147.81, 146.65, 146.25, 141.97, 141.20, 141.11, 140.63, 140.26, 139.89, 139.87, 135.54, 135.24, 135.16, 129.74, 129.30, 129.11, 129.01, 128.31, 128.23, 128.13, 128.05, 127.81, 127.76, 127.58, 127.57, 126.56, 124.27, 123.75, 122.67, 120.92, 115.04, 112.96, 108.05, 35.60, 35.56, 31.78, 31.76, 31.73, 31.61, 31.47, 29.17, 29.12, 29.10, 22.65, 22.62, 13.97. **MS (ESI-TOF):** calcd. for C73H65O3, 1004.5 ; found 1004.7.

Compound **NPI**:

The general Knovenagel procedure is followed with **11** (140 mg, 0.138 mmol), cyanoacetic acid (70.4 mg, 0.828 mmol), ammonium acetate (170.22 mg, 2.21 mmol) and toluene (20 mL). Compound **NPI** is obtained as a green solid (131 mg, 0.121 mmol, 88 %). **^{1}H RMN (THF-d8, 400MHz) δ (ppm):** 8.69 (d, 3J = 8.6 Hz, 1H), 8.52 (d, 3J = 8.1 Hz, 1H), 8.25 (bs, 1H), 8.16 – 7.99 (m, 3J = 8.6 Hz, 3H), 7.76 (bs, 2H), 7.64 – 7.47 (m, 6H), 7.44 (d, 3J = 7.3 Hz, 2H), 7.29 – 7.14 (m, 12H), 7.10 – 6.93 (m, 11H), 6.80 (d, 3J = 9.9 Hz, 1H), 5.94 (d, 3J = 9.8 Hz, 1H), 2.62 (t, 3J = 6.2 Hz, 4H), 1.71 – 1.59 (m, 4H), 1.46 – 1.30 (m, 12H), 0.91 (t, 3J = 6.9 Hz, 6H). **^{13}C RMN (THF-d8, 100MHz) δ (ppm):** 158.1, 149.0, 147.7, 147.2, 145.6, 142.4, 141.2, 141.2, 139.9, 136.8, 132.6, 131.1, 129.2, 129.2, 129.0, 128.6, 128.4, 128.2, 127.9, 126.9, 126.4, 125.31, 124.30, 123.9, 123.7, 123.6, 122.0, 116.5, 82.1, 36.8, 33.1, 33.0, 30.5, 28.2, 23.2, 14.8. **HRMS (MALDI-TOF):** calcd. for $C_{78}H_{68}N_2O_3$, 1080.5224; found 1080.5221

Compound **NPI-ThPh**:

The general Knovenagel procedure is followed with Compound **12** (153 mg, 149.9 µmol, 1.00 eq), cyanoacetic acid (77.4 mg, 0.910 mmol, 6.00eq), ammonium acetate (184.5 mg, 2.39 mmol, 16.0 eq) and toluene (25 mL). Compound **NPI-ThPh** is obtained as a green solid (91 mg, 83.7 µmol, 56%). **^{1}H RMN (THF-d8, 400MHz) δ (ppm):** 8.70 (d, J = 8.4 Hz, 1H), 8.50 (d, J = 8.2 Hz, 1H), 8.20 (br, 1H), 8.14 (d, J = 8.6 Hz, 1H), 8.04 (br, 2H), 7.72-7.58 (m, 5H), 7.58-7.51 (m, 1H), 7.39-7.15 (m, 15H), 7.12-6.95 (m, 12H), 6.79 (d, J = 9.8 Hz, 1H), 6.71 (d, J = 3.1 Hz, 1H), 5.98 (d, J = 9.8 Hz, 1H), 2.62 (dd, J = 17.2, 9.5 Hz, 4H), 1.64 (dt, J = 15.2, 7.5 Hz, 4H), 1.36 (t, J = 12.6 Hz, 12H), 0.95-0.88 (m, 6H). **^{13}C RMN (THF-d8, 100MHz) δ (ppm):** 156.77, 147.80, 147.33, 146.26, 145.87, 143.77, 141.11, 141.08, 139.94, 139.60, 135.27, 129.04, 128.88, 128.74, 128.57, 127.93, 127.86, 127.78, 127.57, 126.29, 126.14, 125.49, 125.40, 123.95, 122.92, 122.50, 122.42, 120.52, 114.78, 79.90, 64.67, 53.88, 35.45, 35.39, 31.78, 31.73, 31.68, 31.55, 29.16, 29.12, 22.54, 22.51, 13.48, 13.43. **HRMS (MALDI-TOF):** calcd. for $C_{76}H_{66}N_2O_3S$, 1086.478; found 1086.478.

Compound **NPI-FuPh**:

The general Knovenagel procedure is followed with Compound **13** (50 mg, 49.8 µmol, 1.00 eq), cyanoacetic acid (25.4 mg, 0.299 mmol, 6.00eq), ammonium acetate (61.4 mg, 0.80 mmol, 16.0 eq) and toluene (5 mL). Compound **NPI-FuPh** is obtained as a green solid (30 mg, 27.9 µmol, 56%). **^{1}H RMN (THF-d8, 400MHz) δ (ppm):** 8.69 (d, J = 8.2 Hz, 1H), 8.51 (d, J = 8.5 Hz, 1H), 8.13 (d, J = 8.5 Hz, 3H), 7.94 (s, 3H), 7.68 – 7.47 (m, 7H), 7.43 – 7.24 (m, 6H), 7.24 – 7.12 (m, 13H), 7.12 – 6.85 (m, 23H), 6.77 (t, J = 9.9 Hz, 4H), 5.93 (d, J = 9.5 Hz, 1H), 2.67 – 2.57 (m, 4H), 1.64 (d, J = 7.5 Hz, 4H), 1.48 – 1.27 (m, 12H), 0.91 (dt, J = 10.1, 5.2 Hz, 6H). **^{13}C RMN (THF-d8, 100MHz) δ (ppm):** 154.89, 145.75, 145.70, 145.44, 144.41, 143.98, 139.90, 139.24, 139.22, 138.09, 137.72, 133.46, 127.89, 127.12, 127.08, 127.03, 126.89, 126.74, 126.59, 126.08, 126.00, 125.91, 125.76, 124.41, 123.54, 122.44, 122.08, 121.79, 121.05, 121.00, 120.64, 120.55, 112.98, 76.42, 62.80, 33.55, 29.91, 29.88,

29.80, 29.71, 27.80, 27.31, 27.28, 22.88, 22.68, 22.48, 22.28, 22.08, 20.69, 20.67, 11.63, 11.61, 11.60. **HRMS (MALDI-TOF):** calcd. for $C_{76}H_{66}N_2O_4$, 1070.501; found 1070.500

II) Solar cells characterisation

A) Solar cells fabrication

TiO2 thin films with a specific thickness and a total area of 0.36 cm2 were screen printed in Solaronix (Switzerland) using a TiO2 nanoparticle paste (Ti-Nanoxide HT/SP). Throughout the manuscript, opaque device refers to a device that includes an additional TiO2 layer of about 3–4 μm in thickness above the mesoporous TiO2 (Solaronix; Ti-Nanoxide R/SP). The active area of the solar cells (0.36 cm2) was estimated from the printing masks and re-measured with a caliper. Beforehand, the electrodes were cleaned with absolute ethanol and dried under an argon flux. These photoanodes were then treated by immersion into a freshly prepared 4.1 mmol.l^{-1} TiO2 aqueous suspension at 70 °C for 20 min. The electrodes were then cooled to room temperature and rinsed with distilled water then absolute ethanol, followed by drying under an argon flux. The electrodes were then sintered under air at 500 °C for 20 min, following the heating procedure reported in Figure S. The photoanodes were then cooled down to 80 °C and sensitized through immersion in the dyeing solution for 16 h at room temperature in the dark ([Dye] = 0.2 M; [chenodeoxycholic acid (CDCA)] = 2.0 M (ratio dye/CDCA = 1/10); CHCl3/tBuOH = 1/1 (vol/vol)). The drilled counter electrodes were coated with a thin layer of platisol (Solaronix) and charred under air at 500 °C using the same heating procedure as presented in Figure S. The sensitized photoanode was rinsed with dichloromethane and absolute ethanol and dried with an argon flux. Both electrodes were then sealed together using a Surlyn thermoglueing polymer (60 μm thick) using a heating press at 105 °C for 16 s. The cell was then filled with an appropriate acetonitrile-based electrolyte (home-made using the following composition: 90 mM of I_2 and 0.5 M LiI) via the pre-drilled hole using a vacuum pump. The

electrolyte injection hole on the counter electrode was then sealed with the aid of Surlyn underneath the thin glass cover using heat. A contact along the cell edges was created.

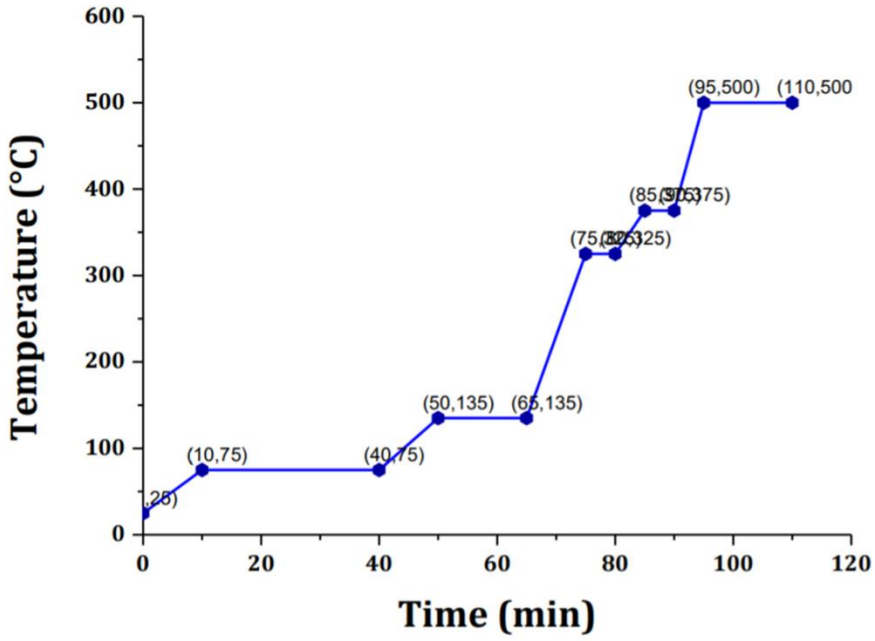

Figure S1: heating procedure for electrode sintering

Before measurements, the AM 1.5 G simulator (Newport class AAA) was calibrated using a reference silicon photodiode equipped with an infrared-cut-off filter (KG3; Schott). This reference photodiode consisted of a readout device and a 2 cm × 2 cm calibrated solar cell made from monocrystalline silicon with a KG3 window. The cell was also equipped with a thermocouple assembled in accordance with IEC 60904-2. The certification is accredited by the National Institute of Standards and Technology to the ISO-17025 standard and is traceable to the National Renewable Energy Laboratory. The current–voltage characteristics of the cells were measured under dark and under the AM 1.5 G (1,000 W m−2) irradiation condition, which was achieved by applying an external potential bias to the cell while measuring the generated photocurrent with a Keithley model 2400 digital source meter. Measurement for the cells was from +0.7 to −0.2 V, divided into 45 points, with a speed of 20 mV s−1. The devices were masked before the measurements to attain an illuminated active area of 0.36 cm2.

B) Impedance spectroscopy

The electrochemical impedance spectroscopy (EIS) measurements were done using an Autolab PGSTAT30 FRA2 potentiostat linked with the NOVA 2.1 software. The studies were carried out on complete solar cells in two different conditions i.e. a) under dark conditions (both device preparation and EIS study) with an applied potential to probe the closed forms of the molecules, and b) under white light illumination after 15 minutes of device activation under 1 Sun (AM 1.5G at 100 mW.cm^{-2}) to probe the photostationary state. The white light measurements were conducted with the applied potential equal to the generated open-circuit voltage under continuous illumination using Thorlabs LED in a wide range of DC light intensities. The impedance spectra (Nyquists and Bode plots) were obtained by applying a 10 mV voltage perturbation in the 10^5 – 10^{-1} Hz frequency range. The main recombination arc appearing at low frequencies, generally 0.1 – 50 Hz, associated with the recombination at the TiO_2 – electrolyte interface, was fitted to an equivalent –RC– circuit element and modelled using the ZView Software (Scribner) to extract the electrical parameters i.e. resistances and capacitances. The recombination resistances and the chemical capacitances are known to depend on the applied potential according to the following equations:

$$R_{ct} \sim exp\left(-\frac{\beta qV}{k_B T}\right)$$

$$C_{\mu} \sim exp\left(\frac{\alpha qV}{k_B T}\right)$$

Where V in the applied voltage, k_B is the Boltzmann constant and T the absolute temperature. The β is the recombination parameter that lies within the 0.5 – 0.8 range and α is the trap distribution parameter in the TiO_2 that lies within 0.15 – 0.35 interval in DSSCs. The recombination resistances and the chemical capacitances fit well to the above equations giving the β and α parameters as shown in Table S1.

Table S1: α and β parameters obtained by impedance spectroscopy

DSSC	α		β	
	Dark	Light	Dark	Light
NPI	0.25	0.23	0.65	0.83
NPI-ThPh	0.26	0.23	0.69	0.86
NPI-FuPh	0.26	0.26	0.67	0.83

Study of **NPI** cells by impedance spectroscopy:

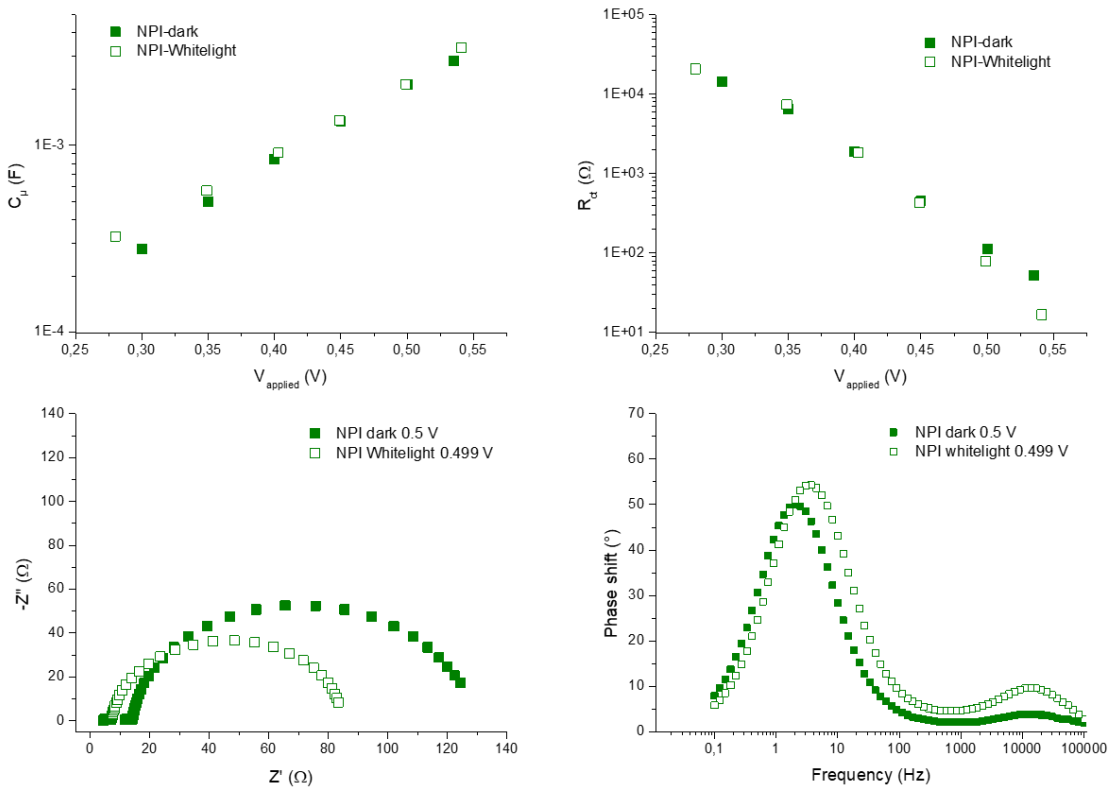

Study of **NPI-ThPh** cells by impedance spectroscopy:

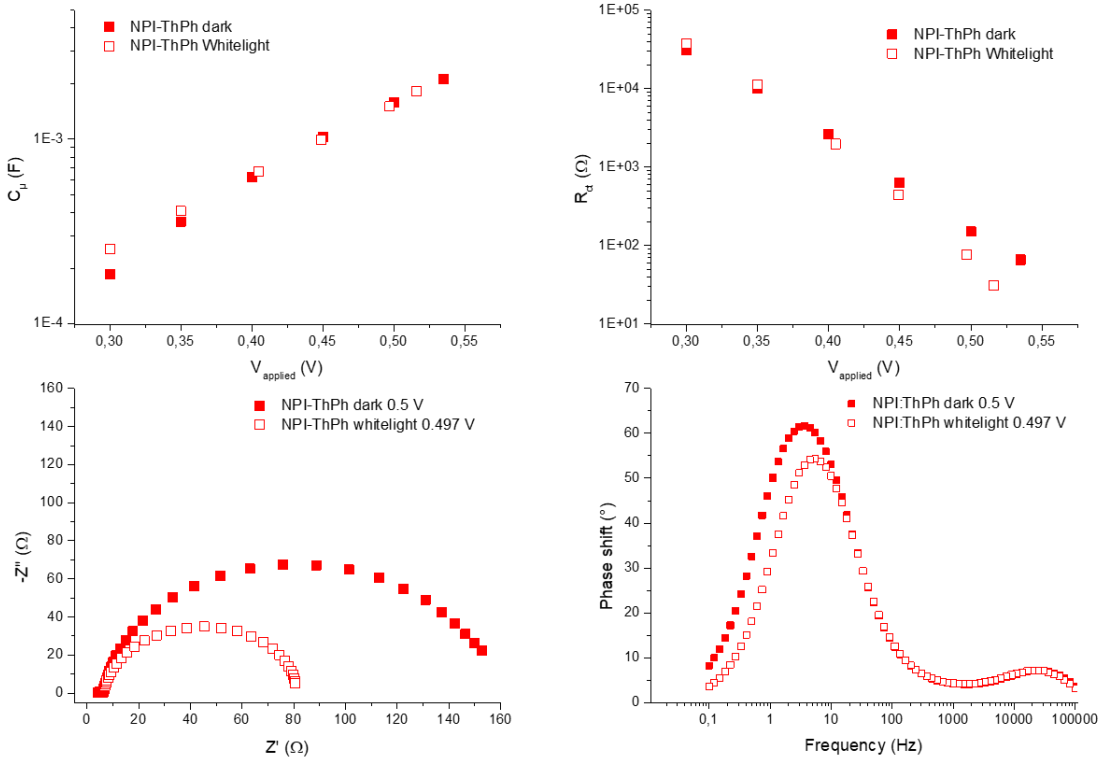

*Figure S6: Study of **NPI-ThPh** cells by impedance spectroscopy*

Study of **NPI-FuPh** cells by impedance spectroscopy:

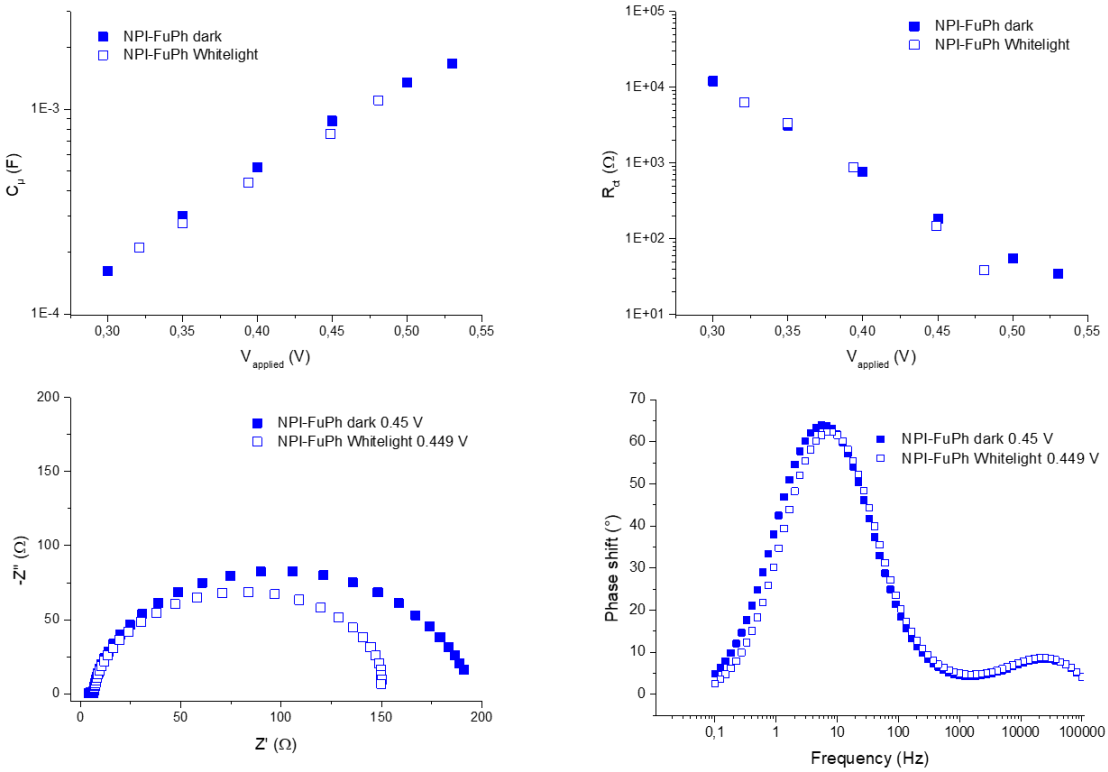

*Figure S7: Study of **NPI-FuPh** cells by impedance spectroscopy*

Comparison between the cells in the dark:

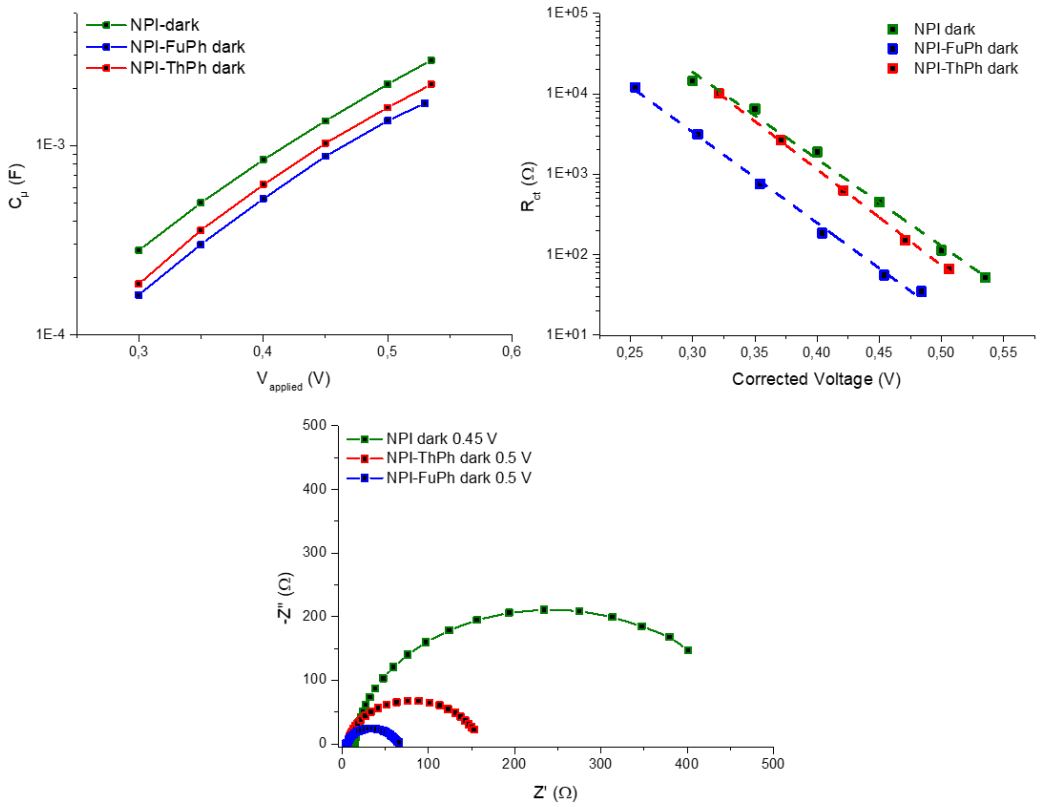

Comparison between the cells under irradiation:

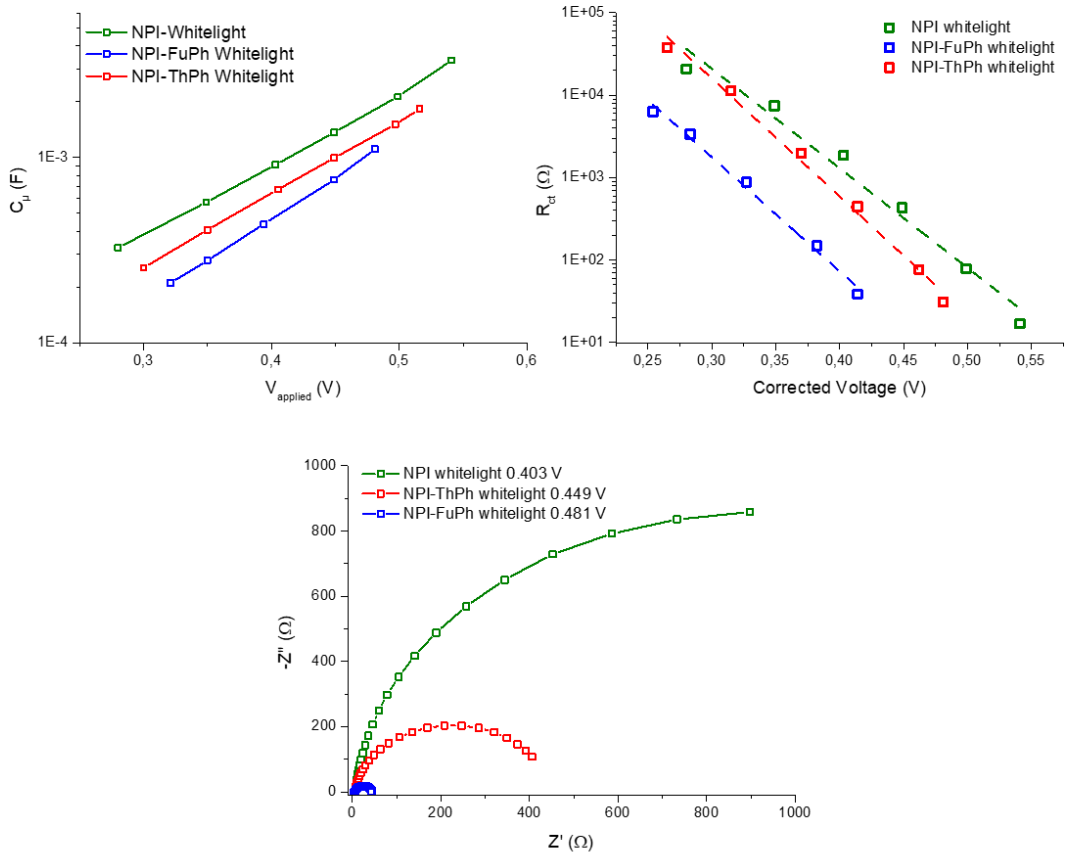

C) IPCE and integrated current

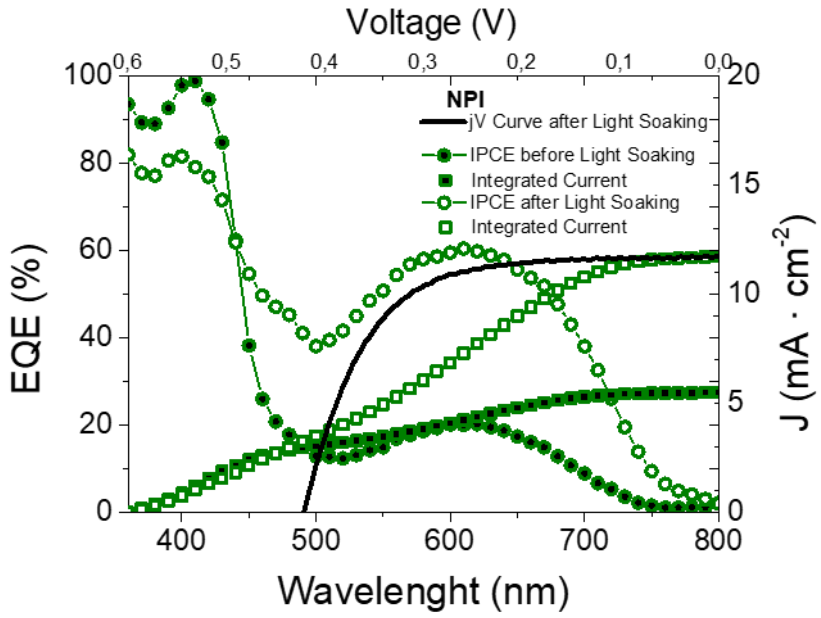

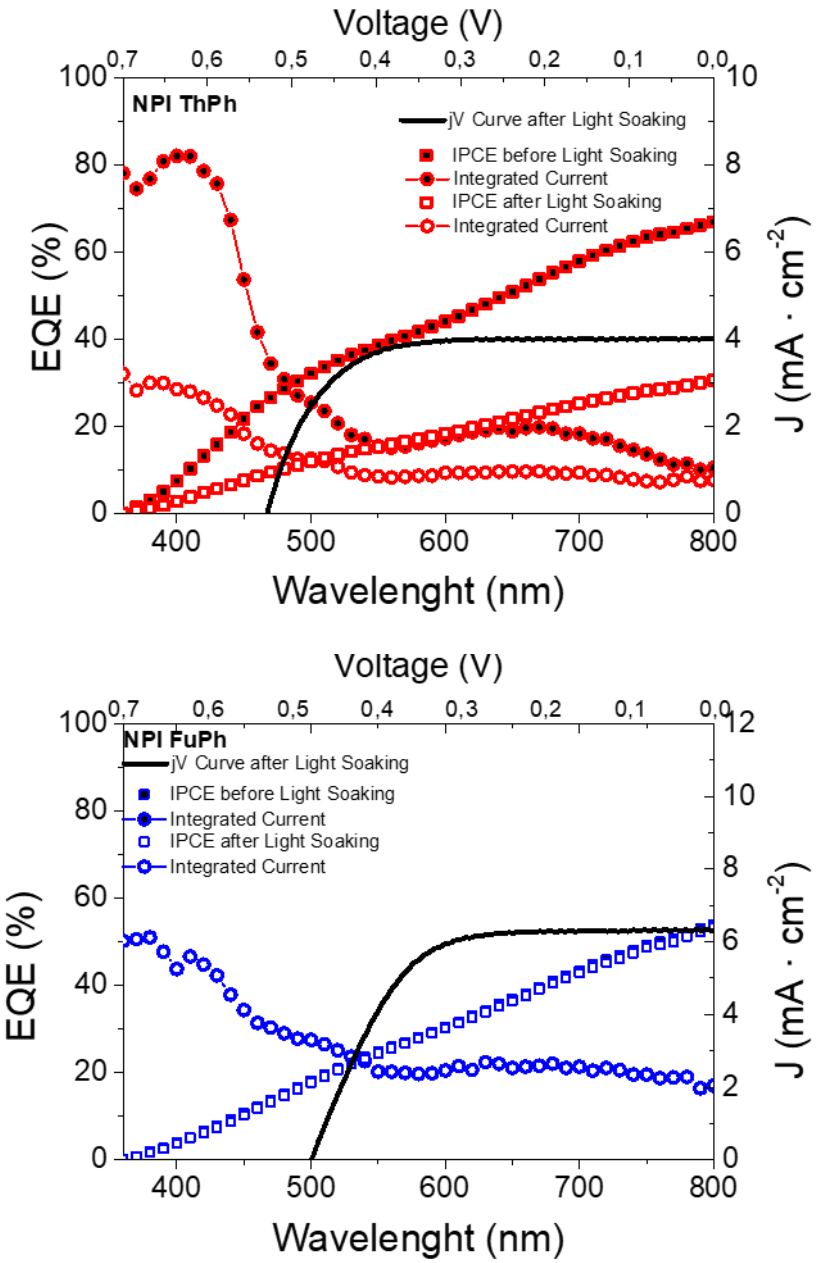

D) Cyclic Voltammetry

The cyclic voltammetry was performed in dichloromethane. The measurements for the closed forms (CF) were performed at room temperature (25 °C). For the opened forms, the measurements were performed at 0 °C after the solution was irradiated at this temperature during 2 minutes. This temperature is used to allow the accumulation of a maximum of dye in its activated state and slow down the discoloration in order to have time to perform the measurement.

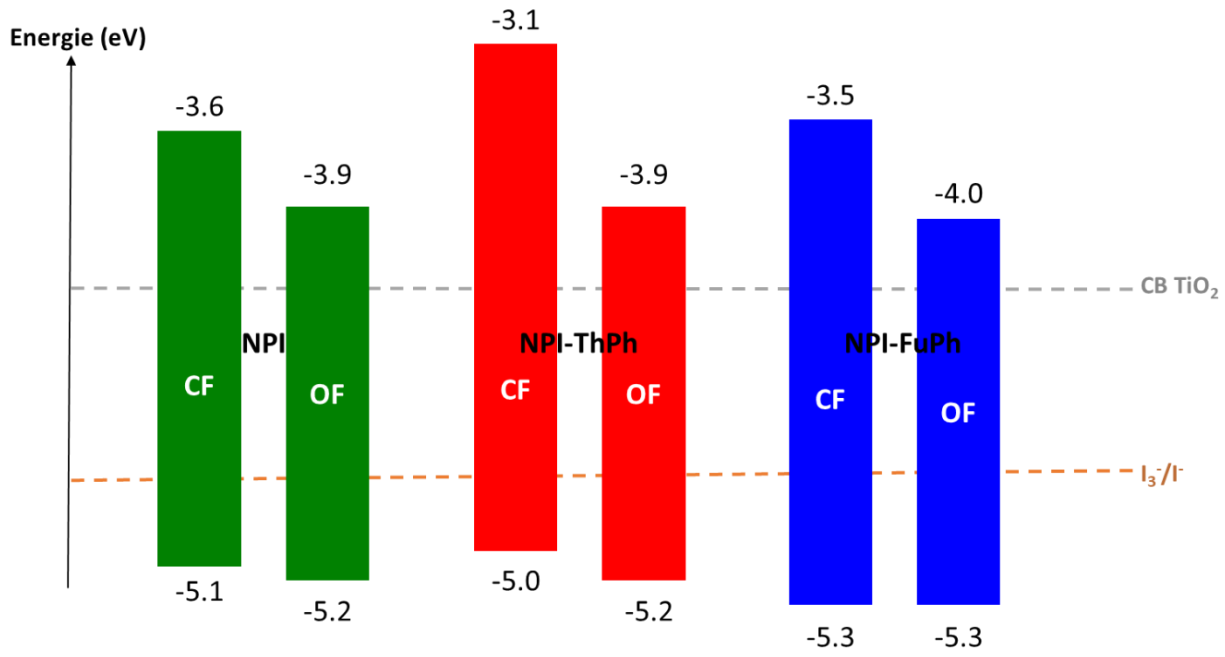

*Figure S10: HOMO-LUMO levels estimated by cyclic voltammetry of **NPI**, **NPI-ThPh** and **NPI-FuPh** in their closed form (CF) and in its opened form (OF). (DCM, $tBAPF_6$, 25 °C for the CF and 0 °C for the OF, 100 $mV.s^{-1}$)*

((Please insert your Supporting Information text/figures here. Please note: Supporting Display items, should be referred to as Figure S1, Equation S2, etc., in the main text…)

III) Computational details

All calculations have been performed in the framework of Density Functional Theory (DFT) using the Orca 4.2 package. [2,3] The hybrid functional B3LYP [4,5] was used for all computations, in combination with the def2-tzvp basis set.[6] Tight criteria for SCF convergence (Grid4 and TightSCF) were chosen. D3BJ Grimme corretion was used.[7] The geometries were optimized with the chosen fonctional in gas phase to obtain the energies of each molecule. The RIJCOSX approximation [8] was used to speed up exchange and Coulomb integrals calculations. The energetic profiles for opening processes were obtained as relaxed energy scans. For the CF – CC opening process scans were run along the elongation of the C-O bond using a 0.01 Å step around the energy maximum. For the CC-CT process, scans were run along the dihedral angle with 0.1 ° steps.

The geometry of the oxydized state of each molecule corresponding to the dye after electron injection were computed using Orca 4.2 package. B3LYP functional was used with the same conditions as mentionned before. The resulting SOMO were modelled and are displayed in Figure S11.

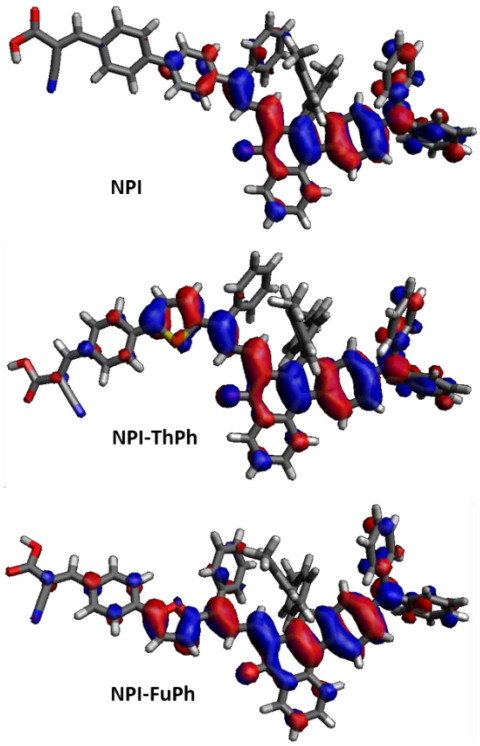

*Figure S11: SOMO modelisation of the oxydized dyes **NPI**, **NPI-ThPh** and **NPI-FuPh**.*

IV) References

[1] Q. Huaulmé, V. M. Mwalukuku, D. Joly, J. Liotier, Y. Kervella, P. Maldivi, S. Narbey, F. Oswald, A. J. Riquelme, J. A. Anta, R. Demadrille, Nat. Energy 2020, 5, 468–477.
[2] F. Neese, WIREs Comput. Mol. Sci. 2012, 2, 73–78.
[3] F. Neese, WIREs Comput. Mol. Sci. 2018, 8, e1327.
[4] A. D. Becke, J. Chem. Phys. 1993, 98, 1372–1377.
[5] C. Lee, W. Yang, R. G. Parr, Phys. Rev. B 1988, 37, 785–789.
[6] F. Weigend, R. Ahlrichs, Phys. Chem. Chem. Phys. 2005, 7, 3297–3305.
[7] S. Grimme, J. Antony, S. Ehrlich, H. Krieg, J. Chem. Phys. 2010, 132, 154104.
[8] F. Neese, F. Wennmohs, A. Hansen, U. Becker, Chem. Phys. 2009, 356, 98–109.